cmgh
CELLULAR AND MOLECULAR GASTROENTEROLOGY AND HEPATOLOGY

ORIGINAL RESEARCH

Liver PP2A-Cα Protects From Parenteral Nutrition-associated Hepatic Steatosis

Gulisudumu Maitiabula,[1,*] Feng Tian,[1,*] Peng Wang,[1] Li Zhang,[1] Xuejin Gao,[1] Songlin Wan,[1] Haifeng Sun,[1] Jianbo Yang,[1] Yupeng Zhang,[1] Tingting Gao,[1] Bin Xue,[2,3,§] Chaojun Li,[2,§] Jieshou Li,[1] and Xinying Wang[1,§]

[1]*Department of General Surgery, Jinling Hospital, Medical School of Nanjing University, Nanjing, China;* [2]*MOE Key Laboratory of Model Animal for Disease Study, Model Animal Research Center of the Medical School of Nanjing University, Nanjing, China; and* [3]*Core Laboratory, Sir Run Run Hospital, Nanjing Medical University, Nanjing, China.*

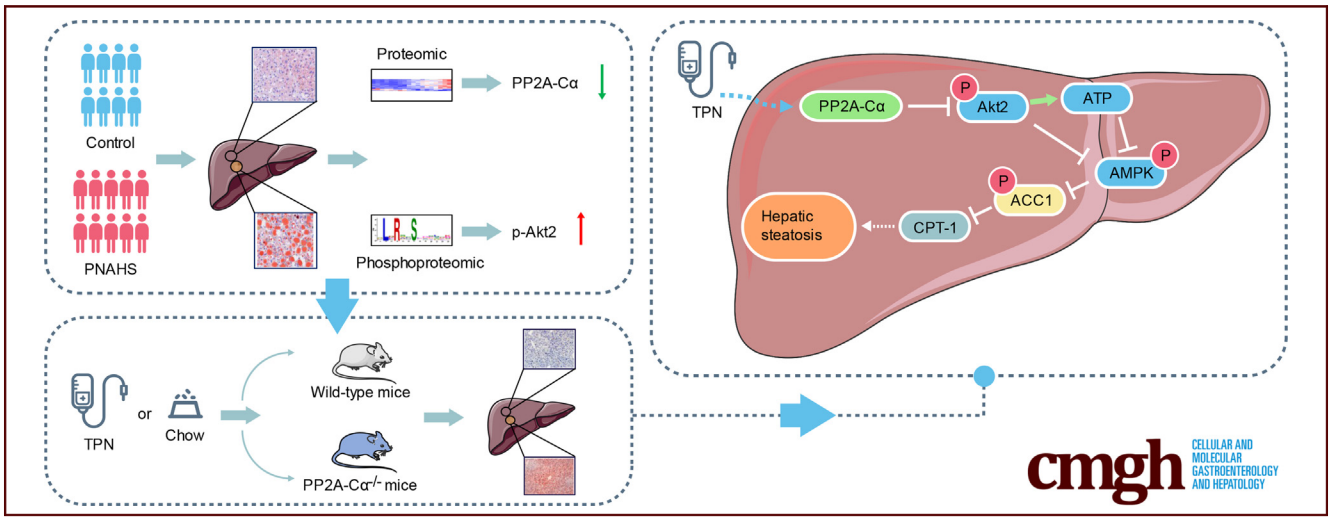

SUMMARY

PP2A-Cα was downregulated in patients and mice with parenteral nutrition-associated hepatic steatosis, concomitant with Akt2 activation. Total parenteral nutrition infusion for 14 days induced hepatic steatosis in dextran sodium sulfate pretreated male mice, and hepatic knockdown of *Ppp2ca* aggravated hepatic steatosis in these mice.

BACKGROUND & AIMS: Parenteral nutrition (PN) is a life-saving therapy for patients with intestinal failure. Hepatic steatosis is a potentially fatal complication of long-term PN, but the involved pathological mechanisms are incompletely unclarified. Herein, we identify the role of protein phosphatase 2A (PP2A) in the pathogenesis of parenteral nutrition-associated hepatic steatosis (PNAHS).

METHODS: Proteomic/phosphoproteomic analyses of liver samples from patients with PNAHS were applied to identify the mechanism of PNAHS. Total parenteral nutrition (TPN) mice model, in vivo, and in vitro experiments were used to assess the effect of PP2A-Cα on liver fatty acid metabolism.

RESULTS: Reduced expression of PP2A-Cα (catalytic subunit) enhanced activation of serine/threonine kinase Akt2 and decreased activation of adenosine monophosphate-activated protein kinase (AMPK) were associated with hepatic steatosis in patients with PNAHS. Mice given PN for 14 days developed hepatic steatosis, down-regulation of PP2A-Cα, activation of Akt2, and inhibition of AMPK. Hepatocyte-specific deletion of PP2A-Cα in mice given PN exacerbated Akt2 activation, AMPK inhibition, and hepatic steatosis through an effect on fatty acid degradation, whereas hepatocyte-specific PP2A-Cα overexpression significantly ameliorated hepatic steatosis accompanied with Akt2 suppression and AMPK activation. Additionally, pharmacological activation of Akt2 in mice overexpressing PP2A-Cα led to the aggravation of hepatic steatosis.

CONCLUSIONS: Our findings demonstrate that hepatic PP2A-Cα serves as a protective factor of PNAHS due to ameliorating hepatic steatosis and improving liver function. Our study provides a strong rationale that PP2A-Cα may be involved in the pathogenesis of PNAHS. *(Cell Mol Gastroenterol Hepatol 2022;14:669–692; https://doi.org/10.1016/j.jcmgh.2022.05.008)*

Keywords: Fatty Acid Degradation; Parenteral Nutrition-associated Hepatic Steatosis; Protein Phosphatase 2A.

See editorial on page 724.

Parenteral nutrition (PN) is a lifesaving therapy for patients with intestinal failure due to insufficient bowel length or function.[1,2] However, long-term PN use carries the risk of developing PN-associated liver disease (PNALD). PNALD is a potentially fatal complication of patients with intestinal failure (IF),[3] which occurs in up to two-thirds of newborns dependent on PN and 15% to 40% of adults with IF receiving long-term PN. Mild-to-moderate hepatic fibrosis and steatosis are evident in 85% and 50%, respectively, of patients receiving long-term PN.[4] Cholestasis and portal inflammation resolve in almost all patients after weaning off PN, whereas portal fibrosis and steatosis persist in 55% and 45% of patients, respectively.[3] Thus, PN-associated hepatic steatosis (PNAHS) is an intractable clinical problem requiring the development of novel therapeutic strategies. Most previous investigations of PNALD have focused on active diseases such as cholestasis and portal inflammation,[5-9] whereas few studies have explored the mechanisms underlying PNAHS.

The serine/threonine kinase Akt is a major mediator in signaling cascades.[10] Several studies have implicated enhanced Akt activity in the pathogenesis of nonalcoholic fatty liver disease (NAFLD).[11,12] Akt2, which is the predominant isoform in the liver,[13] increases hepatic TG accumulation by inhibiting adenosine monophosphate-activated protein kinase (AMPK).[14] Activation of AMPK has been reported to protect against diet-induced obesity, hepatic steatosis, and NAFLD in mice.[15-17] Therefore, Akt2-mediated suppression of AMPK might contribute to the development of PNAHS. Akt is dephosphorylated by protein phosphatase 2A (PP2A),[18,19] a major phospho-serine/threonine phosphatase that regulates cell division, gene regulation, protein synthesis, and cytoskeleton organization.[20] PP2A is a heterotrimer comprising catalytic C-, structural A-, and regulatory B-type subunits.[21,22] The catalytic subunit of PP2A is predominantly encoded by *Ppp2cα* in most tissues, including the liver.[23] Interestingly, pharmacological inhibition of PP2A was found to exacerbate the progression of NAFLD.[24] Based on the available published data, we hypothesized that a decrease in PP2A function might contribute to the pathogenesis of PNAHS through activation of Akt2 and inhibition of AMPK.

In this study, we performed comparative proteomic/phosphoproteomic analyses of liver tissue from patients with PNAHS. We demonstrate for the first time that PNAHS is associated with a reduction in PP2A-Cα expression, an enhancement of Akt2 activity, hepatic TG accumulation, and liver injury in patients and mice. Also, we established a casual role for PP2A-Cα in the liver injury seen in experimental PNAHS using knockout mice with a genetic deletion of PP2A-Cα.

Results

Hepatic Steatosis is Confirmed in Patients With Long-term PN

To investigate the association between PN and hepatic steatosis, the liver pathology of patients received long-term PN has been detected. Computed tomography, hematoxylin and eosin (HE) staining, and oil red O staining (Figure 1, *A-B*) confirmed that patients with PNAHS exhibited increased hepatic lipid deposition when compared with controls (see Table 1 for the clinical characteristics of the participants). Furthermore, the pathological scores for liver steatosis (Figure 1, *C*), aspartate transaminase-to-platelet ratio index (APRI), and Fibrosis-4 index (Figure 1, *D-E*) were higher in the PNAHS group than in the control group. Sirius Red and Masson's trichrome staining (Figure 1, *A*) showed a trend towards liver fibrosis, indicating that long-term PN may accelerate the sequential progression of hepatic steatosis and fibrosis.

PNAHS is Associated With the Decreased Expression of PP2A and Increased Phosphorylation of Akt2

Principal component analysis (Figure 2, *A–B*) and hierarchical clustering (Figure 2, *C–D*) separated the samples from the control and PNAHS groups into 2 clusters. A total of 6811 unique proteins were analyzed, and after correcting for multiple testing by controlling the false discovery rate at 0.05, 998 proteins were significantly differentially expressed (Figure 2, *E*; Supplementary Data 1). The serine/threonine-protein phosphatase 2A catalytic subunit alpha isoform (*Ppp2ca*; fold-change, 0.807; $P = .0001$) and 65-kDa regulatory subunit A beta isoform (*Ppp2r1b*; fold-change, 0.726; $P = .003$) were significantly decreased in the PNAHS group vs the control group (Figure 2, *E*), suggesting that PNAHS is associated with reduced PP2A expression. Kyoto Encyclopedia of Genes and Genomes (KEGG) pathway enrichment analysis revealed that several of the significantly differentiated proteins could be assigned to specific metabolic processes including peroxisome, peroxisome proliferator-activated receptor (PPAR) signaling pathway, fatty acid degradation, citrate (TCA) cycle, and fatty acid metabolism (Figure 2, *F–J*; Supplementary Data 2).

*Authors share co-first authorship; §Authors share co-senior authorship.

Abbreviations used in this paper: ACC1, acetyl-CoA carboxylase-1; AGC, automatic gain control; ALT, alanine aminotransferase; AMPK, adenosine monophosphate-activated protein kinase; APRI, aspartate transaminase-to-platelet ratio index; AST, aspartate aminotransferase; CPT-1, carnitine palmitoyltransferase-1; DSS, dextran sodium sulfate; DTT, dithiothreitol; FGF, fibroblast growth factor; FGFR, fibroblast growth factor receptor; FXR, farnesoid X receptor; HE, hematoxylin and eosin; IF, intestinal failure; KEGG, Kyoto Encyclopedia of Genes and Genomes; MS, mass spectrometry; NAFLD, nonalcoholic fatty liver disease; nano-LC-MS/MS, nanoscale liquid chromatography coupled to tandem mass spectrometry; PCR, polymerase chain reaction; PN, parenteral nutrition; PNAHS, parenteral nutrition-associated hepatic steatosis; PNALD, parenteral nutrition-associated liver disease; PP2A, protein phosphatase 2A; PPAR, peroxisome proliferator-activated receptor; SAMe, S-adenosylmethionine; SDS, sodium dodecyl sulfate; TPN, total parenteral nutrition; TBIL, total bilirubin; TG, triglyceride; TMT, tandem mass tag; WT, wild-type.

Most current article

2352-345X
https://doi.org/10.1016/j.jcmgh.2022.05.008

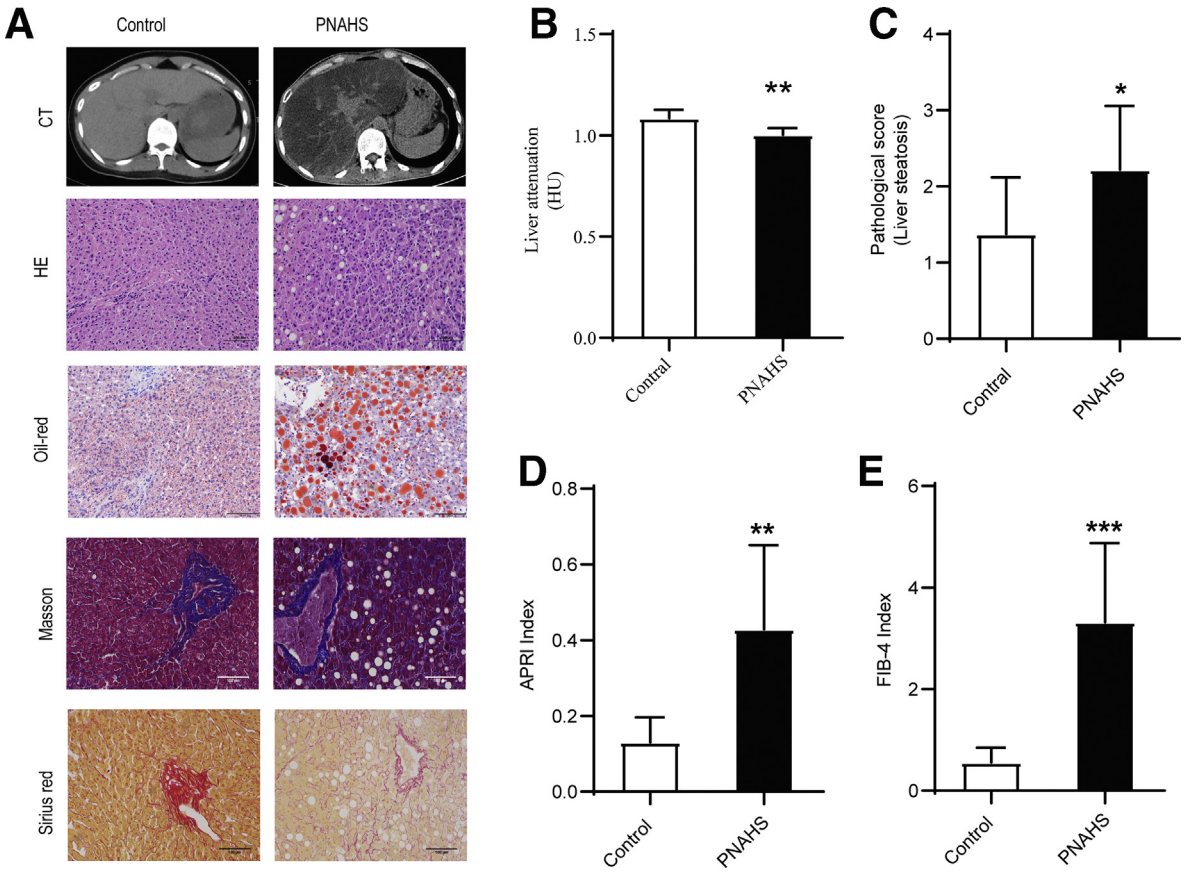

Figure 1. Hepatic steatosis is confirmed in patients with long-term PN. *A*, Representative images showing computed tomography of the liver and liver sections stained with HE, oil red O, Sirius Red and Masson's trichrome obtained from patients with PNAHS or controls. *B*, Hepatic fat content was estimated from the liver attenuation (HU) measured by computed tomography. A lower value of liver attenuation/spleen attenuation indicates a greater hepatic fat content. *C*, Pathological score for liver steatosis determined from the oil red O-stained sections in a blinded manner. *D–E*, The degree of liver fibrosis was estimated from the APRI and Fibrosis-4 index determined from the results of laboratory assessments (AST, ALT, and platelet count). Scores are expressed as mean ± standard deviation (n = 8–10). $^{*}P < .05$; $^{**}P < .01$; $^{***}P < .001$.

In addition, phosphoproteomic analysis identified 5846 phosphorylated proteins, and 1389 sites differed significantly between the PNAHS and control groups after normalization to protein expression levels (Figure 2, *K*; Supplementary Data 3). Among them, 678 phosphorylation sites were up-regulated, and 711 phosphorylation sites were down-regulated. Notably, the phosphorylation of RAC-beta serine/threonine-protein kinase (*AKT2,* fold-change, 1.38) was increased and the phosphorylation of 5'-AMP-activated protein kinase subunit gamma-2 (*PRKAG2*, fold-change, 0.5707) was decreased in patients with PNAHS (Figure 2, *K*). The differentially phosphorylated proteins could be assigned to specific metabolic processes including peroxisome, insulin signal pathway, citrate cycle (TCA cycle), fatty acid metabolism, fatty acid degradation, PPAR signaling pathway, insulin resistance, and AMPK signaling pathway (Figure 2, *L*; Supplementary Data 4).

We combined the protein and phosphoprotein abundances using the Uniprot KB identifier to detect proteins that were up- or down-regulated in both omics' layers. We detected 157 unique proteins that differed significantly in protein abundance and phosphorylation status (Figure 3, *A*). Functional enrichment analysis showed that the up-regulated proteins (Figure 3, *A*, Q2) were most enriched in peroxisome (Figure 3, *B*) and involved in retinol metabolism, PPAR signaling pathway, PI3K−Akt signaling pathway, peroxisome, ferroptosis, fatty acid degradation, carbon metabolism, and AMPK signaling pathway (Figure 3, *C*). These results indicate that PNAHS is associated with decreased expression of PP2A, increased phosphorylation of AKT2, altered AMPK signaling, and fatty acid degradation.

PN for 14 Days Leads to a Downregulation in PP2A-Cα Expression in TPN Mice

Next, we developed a mouse model of TPN-induced hepatic steatosis to investigate the underlying mechanism. Previous research[5,8] indicated that dextran sodium sulfate (DSS)-induced intestinal inflammation and hyperpermeability are necessary for the development of PN-associated liver injury. In our initial experiments, 8-week-old male C57BL/6 mice pretreated with 2.5% DSS to elicit intestinal injury were randomized into 4 groups: chow; PN for 7 days (PN-7); PN for 14 days (PN-14), and PN for 28 days (PN-28). All mice exhibited a decrease in body weight during the first 2 days after surgery followed by a

Table 1. Clinical Characteristics of Patients in the PNAHS and Control Groups

	Control (n = 8)	PNAHS (n = 10)	*P*-value
Gender, M/F	3/5	7/3	.074
Age, *y*	44.25 ± 6.494	46.45 ± 4.902	.7855
BMI, kg/m^2	20.96 ± 0.7736	17.77 ± 0.8208	.0142[a]
TG, *mmol/L*	1.205 ± 0.1596	3.090 ± 0.5412	.0085[b]
ALB, *g/L*	42.18 ± 1.642	35.99 ± 1.514	.0140[a]
TBIL, *μmol/L*	13.05 ± 3.242	36.52 ± 60251	.0084[b]
DBIL, *μmol/L*	4.50 ± 2.168	16.63 ± 3.054	.0072[b]
IBIL, *μmol/L*	8.188 ± 1.978	20.75 ± 5.529	.0697
ALT, *U/L*	33.38 ± 12.14	80.45 ± 21.53	.1043
AST, *U/L*	23.29 ± 5.163	55.36 ± 11.30	.0468[a]
ALP, *U/L*	81.75 ± 25.32	187.5 ± 50.38	.1128
TCHO, *mmol/L*	4.309 ± 0.3181	3.990 ± 0.2924	.4728

Note: All values are presented as the mean ± standard error of the mean.
ALB, Albumin; ALP, alkaline phosphatase; ALT, alanine aminotransferase; AST, aspartate aminotransferase; BMI, body mass index; DBIL, direct bilirubin; F, female; IBIL, indirect bilirubin; M, male; PNAHS, parenteral nutrition-associated hepatic steatosis; TBIL, total bilirubin; TCHO, total cholesterol; TG, triglyceride.
[a]$P < .05$ (Student *t* test).
[b]$P < .01$ (Student *t* test).

progressive increase in body weight, with no significant differences between groups (Figure 4, *A*). However, survival rate was significantly lower in PN-fed mice than in chow mice (Figure 4, *B*). Furthermore, when compared with the EN group, liver mass (relative to body weight) was significantly increased in the PN-14 and PN-28 groups (Figure 4, *C*), muscle mass (relative to body weight) was significantly decreased in the PN-7, PN-14, and PN-28 groups (Figure 4, *D*), and fat mass (relative to body weight) was significantly elevated in the PN-28 group (Figure 4, *E*). Histological examinations of the livers from the PN mice revealed sequential progression of disorganized hepatic cord architecture at 7 days, mild hepatic steatosis at 14 days, and severe hepatic steatosis at 28 days (Figure 4, *F*). When compared with the chow group, the PN-14 and PN-28 groups had significantly higher pathological scores for liver steatosis (Figure 4, *G*). Hepatic TG levels were significantly higher in the PN-7, PN-14. and PN-28 groups than in the chow group (Figure 4, *H*). Furthermore, Serum total bilirubin (TBIL), alanine aminotransferase (ALT), aspartate aminotransferase (AST), and triglyceride (TG) levels increased progressively as the duration of PN was prolonged, with the PN-14 and PN-28 groups having higher levels of all 4 indexes than the chow group (Figure 4, *I-L*). The significantly elevated serum TBIL and AST showed cholestasis and hepatocyte injury.

Subsequently, we evaluated whether PN was associated with changes in phosphorylated Akt2 (p-Akt2, a measure of Akt signaling pathway activity) and PP2A levels. Notably, the PN-14 and PN-28 groups had significantly higher levels of p-Akt2 than the chow group (Figure 5, *A-B*). Moreover, hepatic expression of PP2A protein was significantly lower in the PN-14 and PN-28 groups than in the chow group (Figure 5, *A-B*). Specifically, PP2A-Cα expression in the liver exhibited a dramatic decline, whereas the levels of other PP2A subunits showed only minor alterations (Figure 5, *C*). We observed similar changes in patients with PNAHS (Figure 5, *D*). Collectively, these observations suggest that PN for $\geq$14 days leads to a down-regulation in PP2A-Cα expression that activates Akt2-dependent signaling, and which would likely lead to hepatic steatosis.

Hepatic Knockdown of PP2A-Cα Aggravates PNAHS in C57BL/6J mice

To explore the functional role of PP2A-Cα in PNAHS, we generated liver-specific PP2A-Cα knockout mice (Ppp2ca-LKO) (Figure 6, *A*; Supplementary Table 1) and examined the effects of PN for 14 days in Ppp2ca-LKO mice (Ppp2ca-LKO-PN) and wild-type mice (WT-PN). Compared with WT-PN mice, Ppp2ca-LKO-PN mice exhibited macroscopic changes (fat granule accumulation) and microscopic changes (sections stained with HE or oil red O) consistent with hepatic steatosis (Figure 6, *B*). Ppp2ca-LKO-PN mice also had a significantly higher pathological score for liver steatosis than WT-PN mice ($P < .05$) (Figure 6, *C*). Additionally, the hepatic TG content was significantly elevated in Ppp2ca-LKO-PN mice compared with WT-PN mice (Figure 6, *D*). Furthermore, hepatic steatosis in Ppp2ca-LKO-PN mice was associated with cholestasis and liver dysfunction as evidenced by significant increases in the serum levels of TBIL, ALT, and AST (Figure 6, *E-F*). Western blot analyses confirmed that Ppp2ca-LKO-PN mice had a lower level of PP2A and a higher level of p-Akt2 than WT-PN mice (Figure 6, *H-I*). These data substantiate the proposal that the depletion of PP2A-Cα subunits in hepatocytes leads to the progression of hepatic steatosis in PN mice.

Additional experiments were performed to determine whether adenoviral transduction of PP2A-Cα would

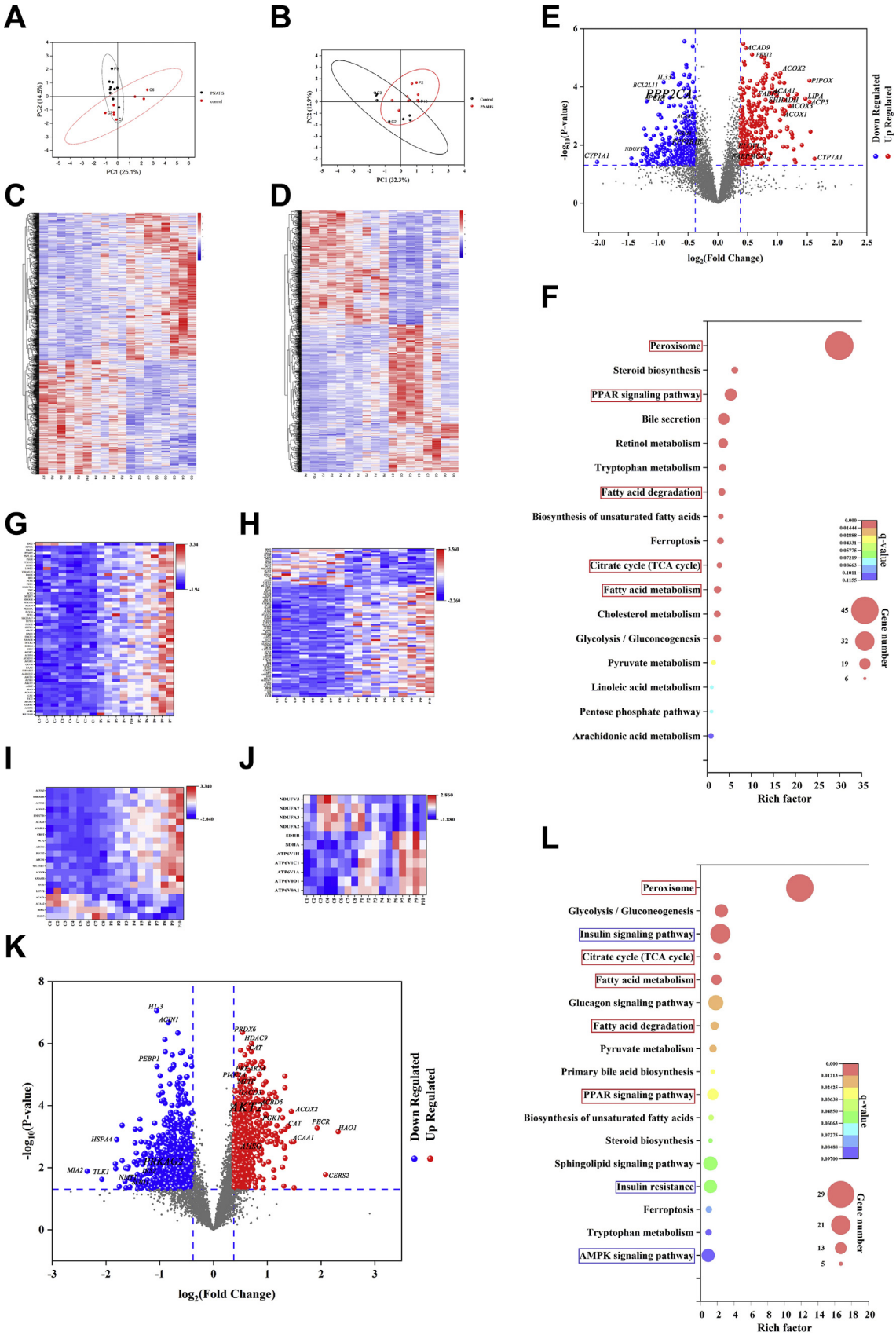
A
PC1 (25.1%)
PC2 (14.5%)
PNAHS
control
B
PC1 (32.3%)
PC2 (12.9%)
Control
PNAHS
C
D
E
PPP2CA
-log10(P-value)
log2(Fold Change)
Down Regulated
Up Regulated
F
Peroxisome
Steroid biosynthesis
PPAR signaling pathway
Bile secretion
Retinol metabolism
Tryptophan metabolism
Fatty acid degradation
Biosynthesis of unsaturated fatty acids
Ferroptosis
Citrate cycle (TCA cycle)
Fatty acid metabolism
Cholesterol metabolism
Glycolysis / Gluconeogenesis
Pyruvate metabolism
Linoleic acid metabolism
Pentose phosphate pathway
Arachidonic acid metabolism
Rich factor
q-value
Gene number
G
H
I
J
K
IKT2
-log10(P-value)
log2(Fold Change)
Down Regulated
Up Regulated
L
Peroxisome
Glycolysis / Gluconeogenesis
Insulin signaling pathway
Citrate cycle (TCA cycle)
Fatty acid metabolism
Glucagon signaling pathway
Fatty acid degradation
Pyruvate metabolism
Primary bile acid biosynthesis
PPAR signaling pathway
Biosynthesis of unsaturated fatty acids
Steroid biosynthesis
Sphingolipid signaling pathway
Insulin resistance
Ferroptosis
Tryptophan metabolism
AMPK signaling pathway
Rich factor
q-value
Gene number

ameliorate PNAHS in C57BL/6J male mice given PN for 14 days. As shown in Figure 7, *A*, PP2A-Cα was uniquely overexpressed in the liver after administration of the adenoviral vector. When compared with controls (adenoviral transduction of GFP followed by PN for 14 days; Ad-GFP-PN group), forced expression of PP2A-Cα (Ad-PP2A-PN group) led to reductions in hepatocyte fat deposition and the pathological score for liver steatosis (Figure 7, *B-C*). The Ad-PP2A-PN group also exhibited significantly lower levels of hepatic TG (Figure 7, *D*), serum TBIL, ALT, and AST (Figure 7, *E-G*). Furthermore, hepatic overexpression of PP2A-Cα was associated with reduced phosphorylation of Akt2 in the liver (Figure 7, *H-I*).

The results indicate that PP2A-Cα can ameliorate PNAHS by reducing the phosphorylation and activation of Akt2. Therefore, we directly examined whether pharmacological inhibition of Akt2 would attenuate PNAHS. Administration of the Akt2 inhibitor MK-2206 alleviated liver steatosis and liver dysfunction in WT-PN mice (Figure 8, *A–F*). Furthermore, MK-2206 reduced the level of p-Akt2 without influencing the level of PP2A-Cα (Figure 8, *G*).

Pharmacological Activation of Akt Causes PNAHS in Mice Overexpressing PP2A-Cα

Because PP2A interacts with and inactivates Akt2 in vitro and in vivo,[25] we explored whether pharmacological activation of Akt2 promoted PNAHS in mice overexpressing PP2A-Cα. Ad-PP2A-PN mice were administered SC79 (20 mg/kg), a selective activator of Akt,[26] by intraperitoneal injection on days 1 and 8 after the PN intervention (Ad-PP2A-PN+SC79). The administration of SC79 to Ad-PP2A-PN mice increased fat deposition in hepatocytes and the pathological score for liver steatosis (Figure 9, *A-B*). The Ad-PP2A-PN+SC79 group also had significantly higher levels of hepatic TG, serum ALT, and serum AST (Figure 9, *C-E*) than mice in the Ad-PP2A-PN group. Western blot analyses confirmed that SC79 enhanced Akt2 activation but not PP2A-Cα protein expression (Figure 9, *F*). The findings imply that pretreatment with SC79 prevents the inhibitory effects of PP2A-Cα on PNAHS, further supporting the hypothesis that PP2A-Cα suppresses PNAHS in mice by reducing Akt2 activation.

Hepatic Knockdown of PP2A-Cα Suppresses Hepatic Fatty Acid β-Oxidation Through Akt2- and AMPK-dependent Pathways

Finally, we explored whether the effects of PP2A-Cα on PNAHS might be mediated through alterations in hepatic lipid metabolism. The mRNA expression of enzymes related to fatty acid metabolism such as carnitine palmitoyl transferase 1A (CPT-1) and acetyl-CoA acetyltransferase were significantly decreased in WT-PN and Ppp2ca-LKO-PN mice (Figure 10, *A-D*). These results were consistent with our omics results, which showed that the differentially expressed proteins were enriched in PPAR signaling pathway and fatty acid degradation (Figure 2, *F, L*).It has been reported that Akt maintains energy homeostasis by retaining the cellular ATP level so as to inhibit AMPK activity,[27] which increases the activity of CPT1 (a key enzyme in the hepatic β-oxidation of long-chain fatty acids). The import of fatty acids into mitochondria for β-oxidation relies on a transport system that requires CPT1. Malonyl CoA, which is generated by acetyl-CoA carboxylase-1 (ACC1) and ACC2, is a potent inhibitor of CPT1. AMPK phosphorylates and inhibits ACC to decrease the malonyl CoA pool, which in turn reduces lipid synthesis and increases fatty acid uptake by mitochondria for β-oxidation.

First, we explored whether PP2A-Cα influenced the intracellular ATP level in the liver. When compared with WT mice given PN for 14 days, hepatic ATP level was significantly increased in Ppp2ca-LKO mice and significantly decreased following overexpression of PP2A-Cα (Figure 10, *E*). In vitro experiments in AML12 cells showed that inhibition of PP2A with LB100 increased the levels of TG and ATP, whereas inhibition of Akt with MK-2206 had the opposite effects (Figure 10, *F-G*). Notably, AMPK activity as measured by its phosphorylation at Thr-172 was significantly lower in mice given PN for 14 days than in chow mice (Figure 11, *A*). This reduction in AMPK activity in PN-treated mice was associated with decreased phosphorylation of ACC1 at Ser-79 (ie, enhanced ACC activity) (Figure 11, *A*), as might be expected given that Ser-79 is the target of AMPK, as well as reduced CPT-1 expression (Figure 11, *A*), which was secondary to a build-up of malonyl CoA (Figure 11, *B*).

Figure 2. (*See previous page*). Proteomic and phosphoproteomic analysis of liver between patients with PNAHS (n = 10) and controls (n = 8). *A–B*, Principal component analysis scatter plots. The horizontal coordinate PC1 and vertical coordinate PC2 respectively represent the scores of the first and second principal components. Each scatter represents a sample, and the color and shape of the scatter represent the 95% confidence intervals (Hoteling's T-squared ellipse) of different grouped samples. *C–D*, Heat maps of representative proteins/phosphosites significantly altered among the 2 groups. Colored boxes represent upregulation (*red*) and downregulation (*blue*) in the PNAHS group. The color scale (upper-right) indicates the fold-change in protein/phosphosite expression for all samples. *E, K*, Volcano plots showing the *P*-value (y-axis) and fold-change (x-axis) of the quantified proteins/phosphosites identified in the proteomic and phosphoproteomic analyses (the proteins/phosphosites that showed significant downregulation and upregulation are reported in *blue* and *red*, respectively). F, L, Bubble diagrams showing the KEGG metabolic pathway enrichment analyses for the proteome/phosphoproteome. The horizontal axis shows the Rich factor (degree of enrichment), and the vertical axis shows the KEGG pathway information. The size of the circle represents the number of differentially expressed peptide-dependent proteins in the mapping pathway: the larger the circle, the greater the number of peptide-dependent proteins. The color of the circle indicates the magnitude of the corrected *P*-value: the redder the color, the smaller the *P*-value. The metabolic pathways enriched in both the proteome and phosphoproteome are circled in *red*, and the metabolic pathways enriched only in the phosphoproteome are circled in *blue*. *G–J*, Heat maps of the proteins significantly altered among the 2 groups that were associated with peroxisome, fatty acid metabolic processes, fatty acid catabolic processes, and oxidative phosphorylation, respectively. Colored boxes represent upregulation (*red*) and downregulation (*blue*) in the PNAHS group. (PNAHS, n = 10; control, n = 8).

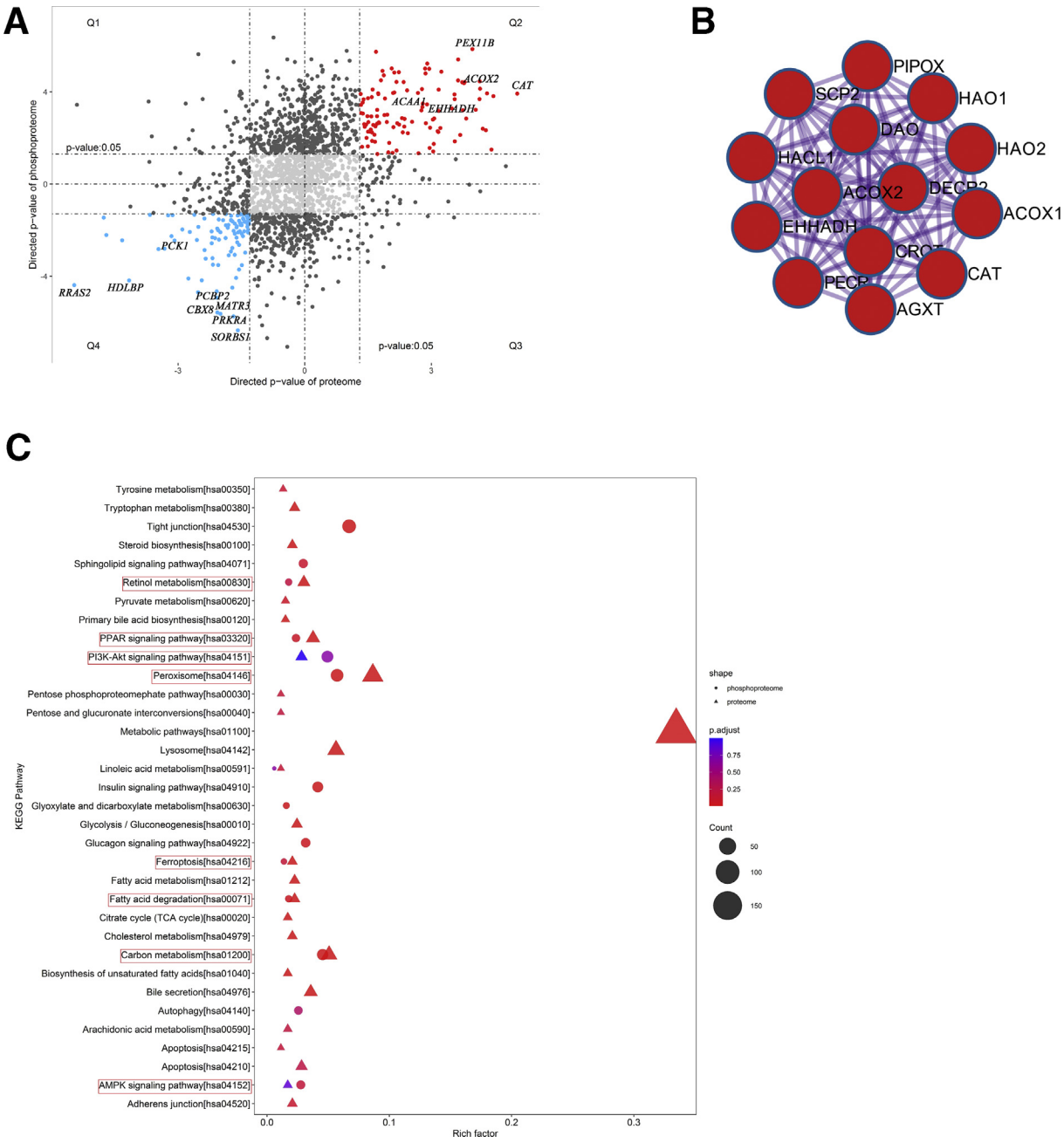

Figure 3. Proteome–phosphoproteome correlation. *A*, Proteome–phosphoproteome comparison. Q1, Q2, Q3, and Q4 mark the quadrants of the correlation plots. *B*, Protein–protein interaction analysis of the proteins that differed significantly in protein abundance and phosphorylation status. *C*, KEGG metabolic pathway enrichment analysis in the proteome and phosphoproteome. The lipid metabolism-associated pathways are circled in *red*. (PNAHS, n = 10; control, n = 8).

Furthermore, forced expression of PP2A-Cα completely reversed the effects of PN on AMPK activity, ACC1 activity, malonyl CoA concentration and CPT-1 protein expression (Figure 11, *C*). In addition, pharmacological stimulation of Akt2 activity with SC79 counteracted the effects of PP2A-Cα overexpression on AMPK activity (Figure 11, *D*) and hepatic ATP level (Figure 10, *H*).

We further investigated the role of AMPK in PNAHS using the AMPK activator GSK621. The results of histological examination, biochemistry analyses, and Western blotting experiment indicated that PN-induced lipid deposition and hepatocellular damage in mice were alleviated upon treatment with the AMPK activator (Figure 12, *A*–*G*).

These results suggest that PN leads to a reduction in PP2A-Cα expression that stimulates Akt2 to inhibit AMPK activity in mice. This PN-associated inhibition of AMPK function would be expected to enhance de novo synthesis of fatty acids and reduce β-oxidation of fatty acids, with the resulting enhancement of hepatic fatty acid levels likely contributing to the development of hepatic steatosis.

In this study, the regulator of PP2A-Cα expression is unknown. Fibroblast growth factor 15 (FGF15) is the mouse

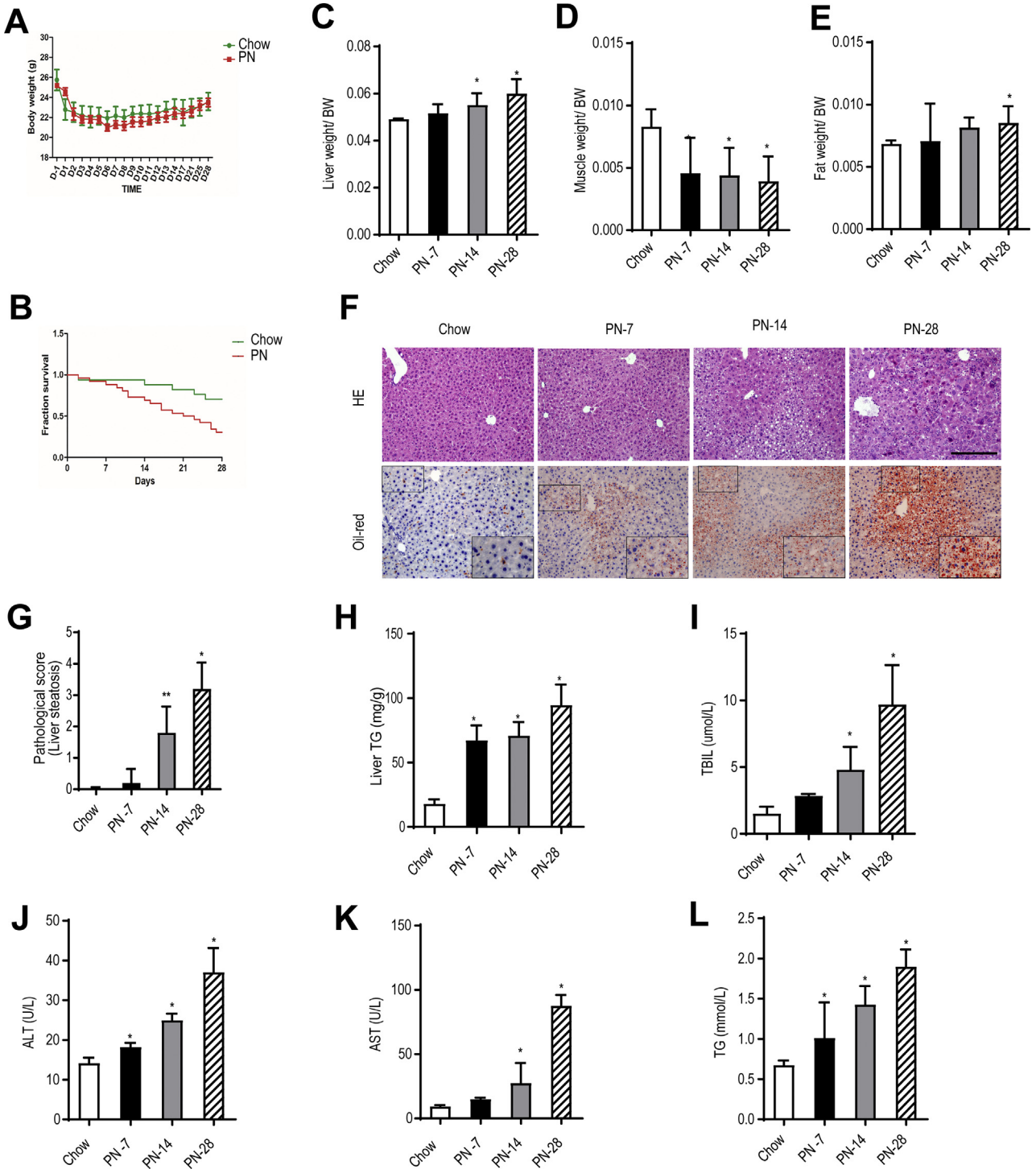

Figure 4. The PN-14-day mice exhibited hepatic steatosis. *A*, The body weights of mice in the chow group and PN group were measured every 2 days. *B*, Survival fraction for mice in the chow and PN groups. *C–E*, Liver mass, muscle mass, and epididymal fat mass relative to bodyweight for mice in the chow and PN groups at the indicated time points. *F*, Representative images showing liver sections stained with HE or oil red O (200× magnification) from mice in the chow, PN-7, PN-14, and PN-28 groups. *G*, Pathological scores for hepatic steatosis determined from HE-stained sections in a blinded manner. *H*, TG levels in liver homogenates from mice in the chow, PN-7, PN-14, and PN-28 groups. *I–L*, Serum TBIL, ALT, AST, and TG levels in mice from the chow, PN-7, PN-14, and PN-28 groups. Scores are expressed as mean ± standard deviation (n = 5–7). $^{*}P < .05$; $^{**}P < .01$.

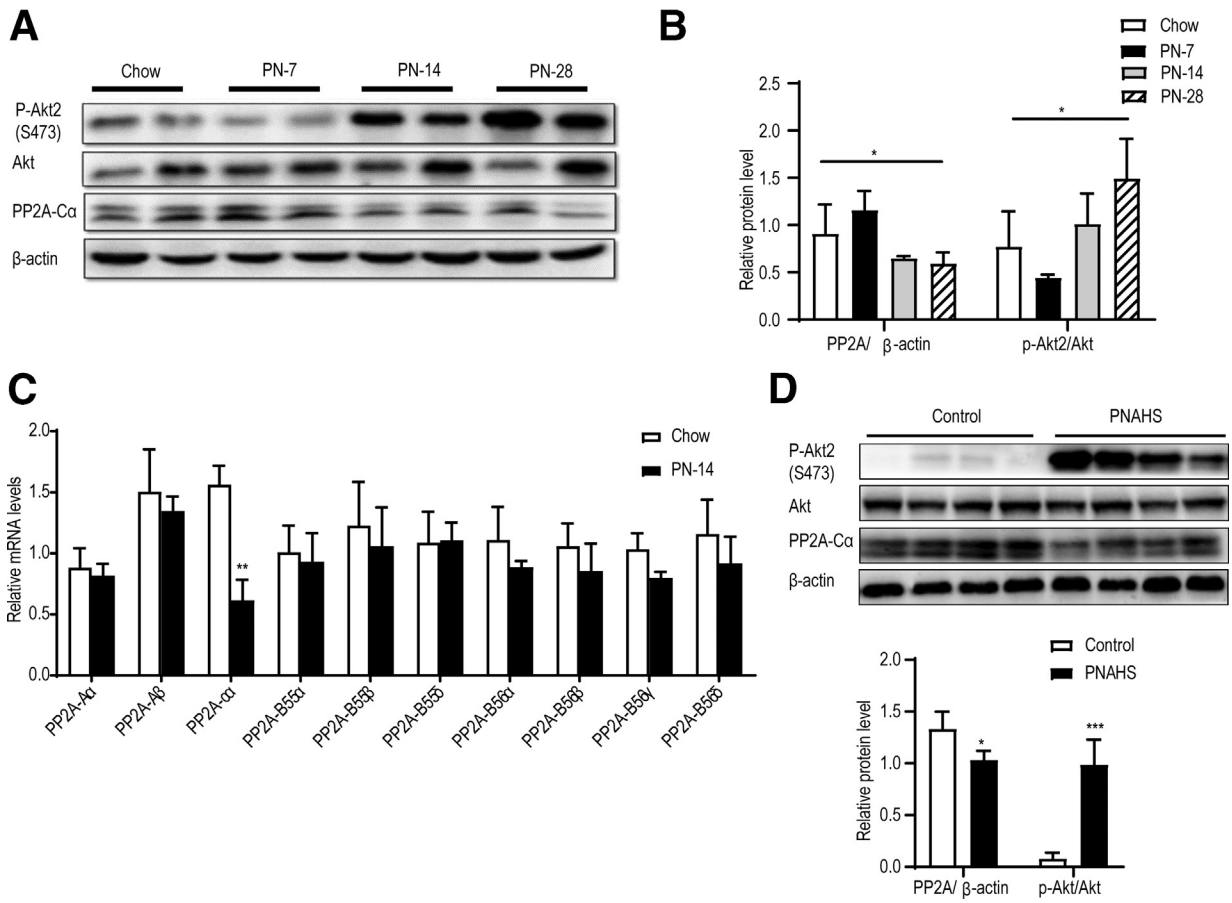

Figure 5. PP2A-Cα was downregulated in mice and patients with PNAHS. *A–B*, Western blot analyses and densitometric quantification of the expression levels of various proteins of interest in mice. *C*, Hepatic mRNA expression levels of the Aα, Aβ, B55α, B55β, B55δ, B56α, B56β, B56γ, and B56δ subunits of PP2A in mice from the chow and PN-14 groups. *D*, Western blot analyses and densitometric quantification of the expression levels of various proteins in patients with PNAHS and controls. The results are expressed as the mean ± standard deviation (n = 5–7 mice/group, n = 8–10 patients/group). **P* < .05; ***P* < .01; ****P* < .001.

ortholog of human FGF19.[28] FGF15/FGF19 are induced by the bile acid-activated nuclear receptor farnesoid X receptor (FXR), and known to be predominantly expressed in the small intestine, gallbladder, brain, cartilage, skin, and kidney.[29] Secreted FGF15/19 reaches the liver via the portal vein, where it binds fibroblast growth factor receptor 4 (FGFR4)[30] and activates signaling pathways that inhibit bile acid synthesis by suppressing Cyp7a1 and Cyp8b1g gene expression.[31]

Previous studies demonstrated that FGF15/19 were involved in the inhibition of hepatic bile acid synthesis[32] and played physiological roles in liver fat metabolism.[33,34] Available studies support the hypothesis that altered FXR signaling is important in the onset of parenteral nutrition-associated cholestasis.[35,36] Moreover, serum FGF19 concentration was associated with hepatic portal inflammatory and fibrotic liver changes in patients with pediatric intestinal failure.[6] Our proteomic results indicated that FXRα (Nr1h4, fold-change = 0.76) was downregulated in patients with PNAHS (Supplementary Data 1), and cholesterol 7a-hydroxylase (CYP7A1; fold-change = 3.08) and sterol 12a-hydroxylase (CYP8B1; fold-change = 1.52), which are the rate-limiting enzymes in the conversion of cholesterol to primary bile acids, were strongly upregulated in patients with PNAHS (Supplementary Data 1). Therefore, we hypothesized that FGF15/19 is involved in PP2A-Cα-mediated hepatic steatosis. Western blotting was used to detect FGF19, FXR, and FGFR4 expression in hepatic tissue of patients with PNAHS. Consistent with the proteomics results, FXR and FGFR4 protein expressions were decreased in patients with PNAHS. However, there were no significant differences in liver FGF19 protein levels between the control and PNAHS groups (Figure 13, *A-B*).

We further examined liver FGF15, FXR, and FGFR4 protein expression in the chow, PN-14, Ppp2ca-LKO-PN, and Ad-PP2A-PN mice. The results revealed that liver FXR and FGFR4 levels were decreased in PN mice, but there were no significant differences in liver FGF15 protein expression (Figure 13, *C-D*). To confirm these results, immunohistochemistry was used to observe the FGF15 protein in liver. Consistent with the Western blotting results, immunohistochemistry results showed that there were no significant differences in liver FGF15 protein expression between the chow and PN mice (Figure 13, *E*). Notably, the deletion or overexpression of PP2A

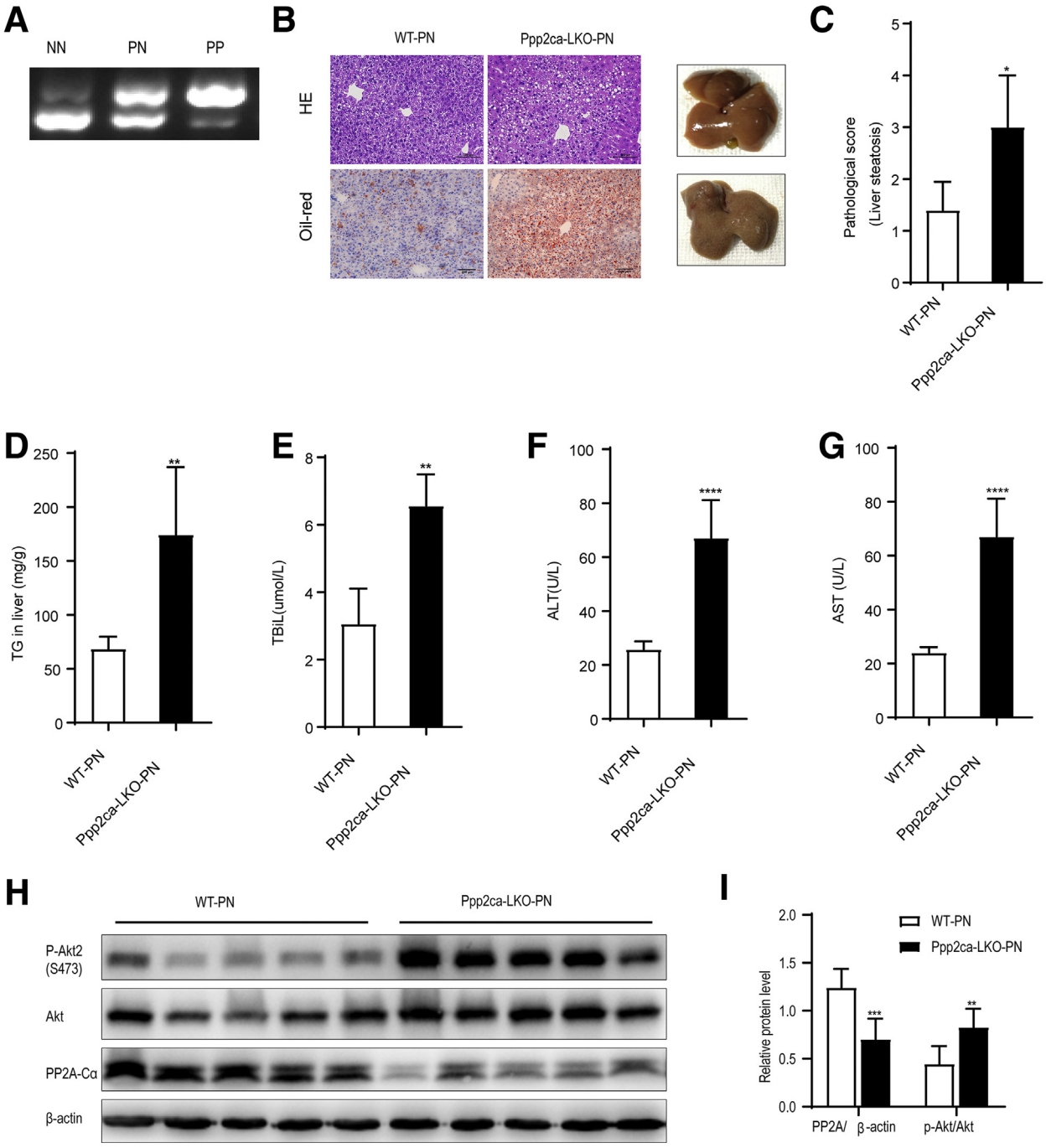

Figure 6. Conditional deletion of *Ppp2ca* aggravates hepatic steatosis in mice given PN. *A*, DNA genotyping (PCR) in wild-type (NN), heterozygote (PN), and homozygote (PP) mice. *B*, Representative images showing liver sections stained with HE or oil red O from mice in the WT-PN group (WT mice given PN) and Ppp2ca-LKO-PN group (mice with conditional knockout of Ppp2ca given PN). *C*, Pathological scores for hepatic steatosis from oil red O in a blinded manner. *D*, TG levels in liver homogenates from mice in the WT-PN and Ppp2ca-LKO-PN groups. *E–G*, Serum TBIL, ALT, and AST levels in mice from the WT-PN and Ppp2ca-LKO-PN groups. *H–I*, Western blot analyses and densitometric quantification of the expression levels of various proteins. The results are expressed as the mean ± standard deviation (n = 7). **P* < .05; ***P* < .01; ****P* < .001; *****P* < .0001.

did not alter FXR or FGFR4 protein expression in PN mice. These results indicated that the effects of PP2A-Cα on PNAHS are not dependent on FGF15/19. We detected liver S-adenosylmethionine (SAMe), which is a critical regulator of PP2A activity, in mice.[37] As expected, SAMe was dramatically reduced in PN mice compared with control mice (Figure 13, *F*). Moreover, PP2A-Cα and Akt2 intervention did not affect SAMe levels in the liver (Figure 13, *F*). These results indicate that low liver SAMe levels in PNAHS mice decrease PP2A expression and activity, which contributes to hepatic steatosis.

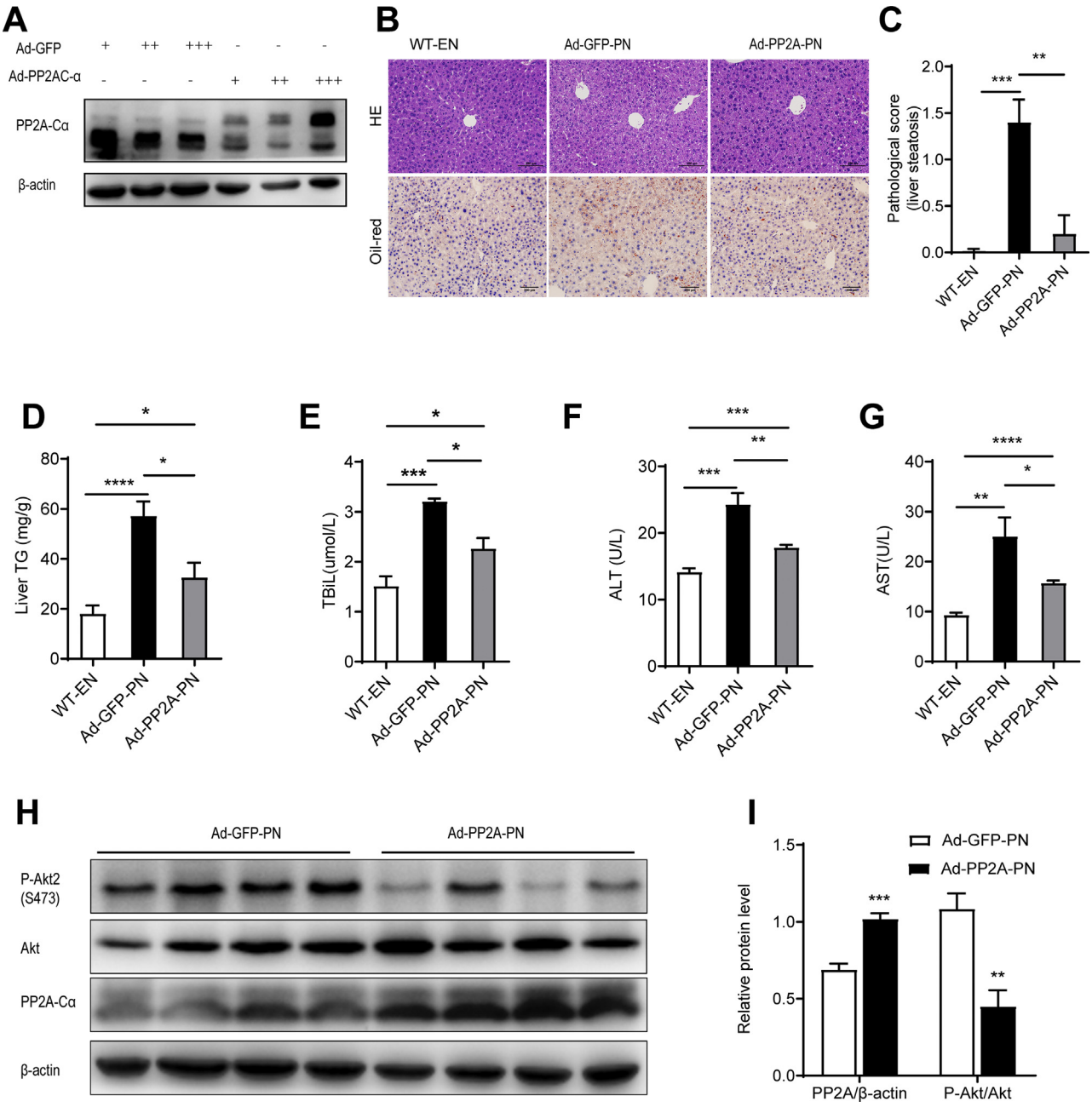

Figure 7. Hepatic overexpression of PP2A-Cα can ameliorate PNAHS. *A*, AML12 cells were infected with Ad-GFP or Ad-PP2A, and PP2A-Cα levels were detected by Western blots. *B*, Representative images showing liver sections stained with HE or oil red O from mice in the chow, Ad-GFP-PN group (control mice transfected with green fluorescent protein and given PN) and Ad-PP2A-PN group (mice transfected with Ppp2ca and given PN). *C*, Pathological scores for hepatic steatosis determined from oil red O sections in a blinded manner. *D*, TG levels in liver homogenates from mice in the chow, Ad-GFP-PN, and Ad-PP2A-PN groups. *E–G*, Serum TBIL, ALT, and AST levels in mice from the chow, Ad-GFP-PN, and Ad-PP2A-PN groups. *H–I*, Western blot analyses and densitometric quantification of the expression levels of various proteins. The results are expressed as the mean ± standard deviation (n = 5–7). **P* < .05; ***P* < .01; ****P* < .001; *****P* < .0001.

Discussion

The present study demonstrates for the first time that PNAHS in human patients is associated with a down-regulation of hepatic PP2A-Cα expression and an increase in Akt2 phosphorylation. Studies in mice model of PNAHS revealed that a reduction in PP2A-Cα expression led to enhanced Akt2 activity that inhibited AMPK. PN-associated inhibition of AMPK would be expected to suppress fatty acid degradation, increase hepatic TG accumulation, and promote steatosis.

Hepatocyte-specific deletion of *Ppp2r1a* promotes liver fibrosis,[38] implicating PP2A involvement in liver injury. However, the role of PP2A in PNAHS remains unclarified. Although pharmacological inhibition of PP2A aggravated

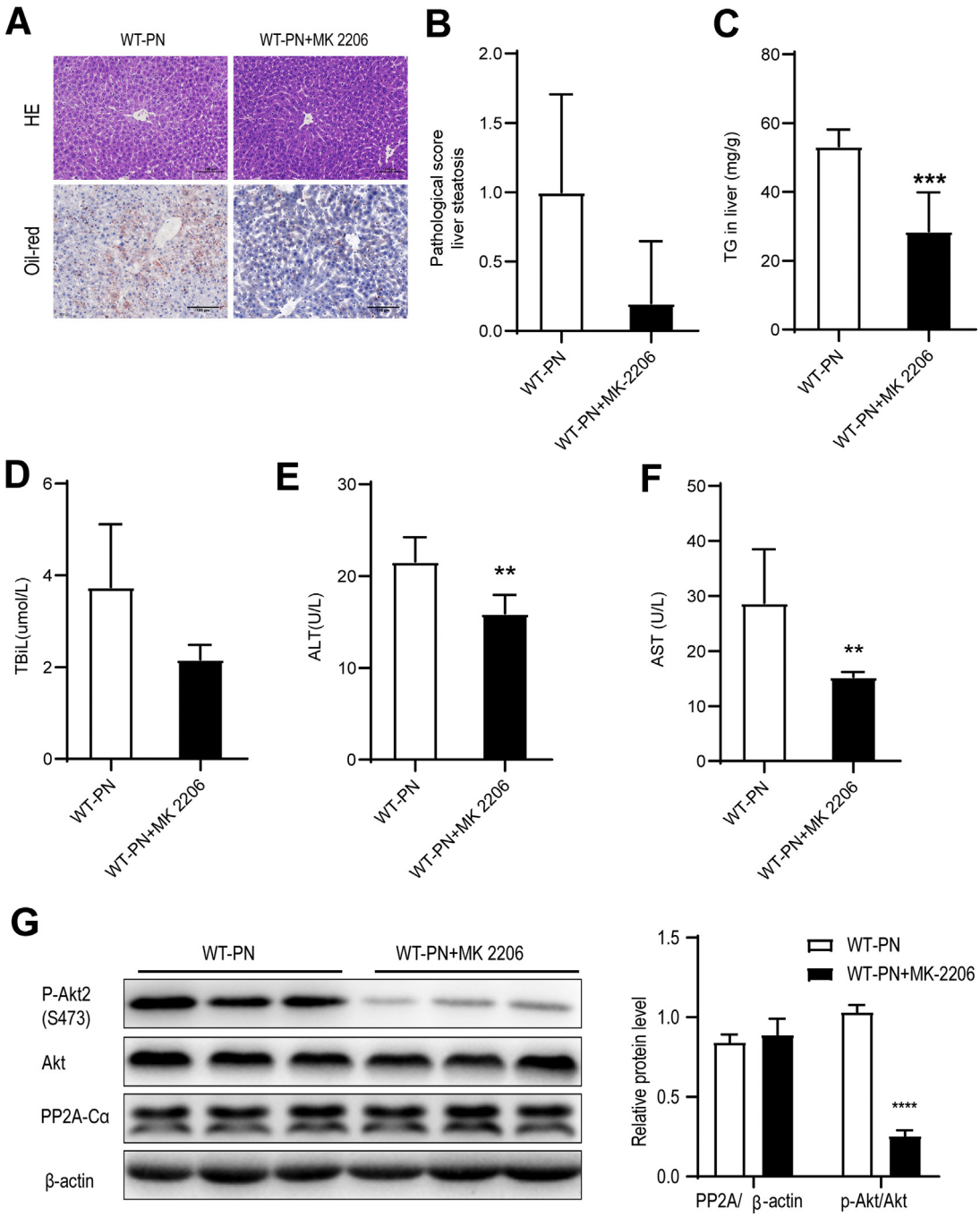

Figure 8. Pharmacological inhibition of Akt2 attenuates PNAHS and liver dysfunction in mice. *A*, Representative images showing liver sections stained with HE or oil red O from mice given PN and either treated (WT-PN+MK 2206 group) or untreated (WT-PN group) with the Akt inhibitor MK-2206. *B*, Pathological scores for hepatic steatosis determined from oil red O sections in a blinded manner. *C*, TG levels in liver homogenates from mice in the WT-PN group and WT-PN+MK 2206 group. *D–F*, Serum TBIL, ALT, and AST levels in mice from the WT-PN group and WT-PN+MK 2206 group. *G*, Western blot analyses and densitometric quantification of various proteins of interest. The results are expressed as the mean ± standard deviation (n = 7). $^{**}P < .01$; $^{***}P < .001$; $^{****}P < .0001$.

NAFLD in one study,[24] liver-specific deletion of *Ppp2cα* enhanced glucose metabolism, improved insulin sensitivity, and prevented hepatic TG accumulation in another study.[39] Moreover, inhibition of PP2A with LB100 ameliorated high-fat diet-induced steatosis by modulating hepatic lipogenesis and fatty acid oxidation via AMPK/Sirt1 signaling.[40] Additionally, PP2A deactivation has been implicated in the reversal of fructose-induced NAFLD in mice administered Lactobacillus rhamnosus GG.[41] However, the latter 3 studies focused on liver injury from causes other than PN. The present study clarifies the role of PP2A in PNAHS. Our proteomic analysis showed that *Ppp2ca* and *Ppp2r1b* were

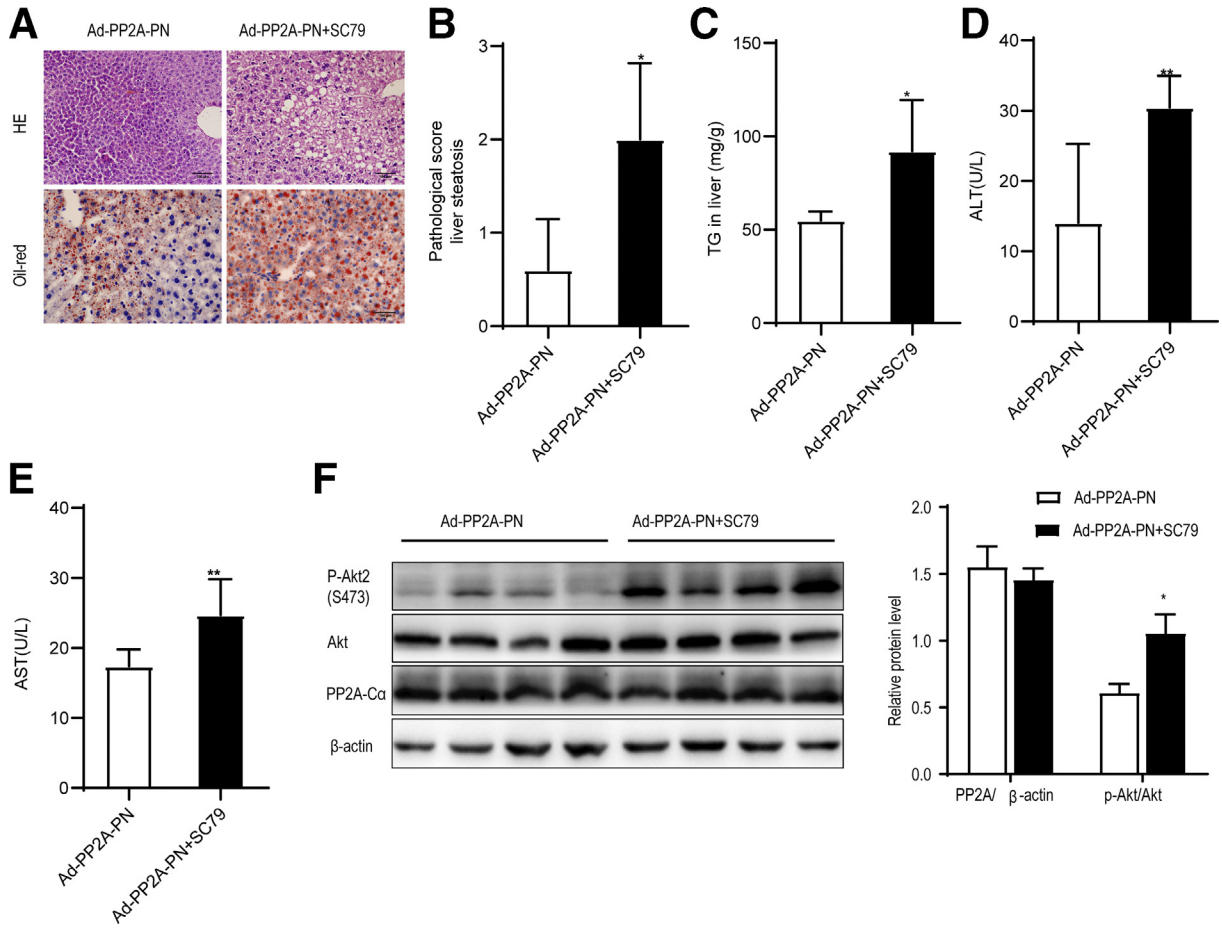

Figure 9. Akt2 hyperactivation abrogates the benefits of protein phosphatase-2A (PP2A) in mice given parenteral nutrition. *A*, Representative images showing liver sections stained with HE or oil red O from mice in the Ad-PP2A-PN group (mice transfected with *Ppp2ca* and given PN) and Ad-PP2A-PN+SC79 group (also treated with 20 mg/kg/week SC79, an activator of Akt). *B*, Pathological scores for hepatic steatosis determined from oil red O sections in a blinded manner. *C*, TG levels in liver homogenates from mice in the Ad-PP2A-PN and Ad-PP2A-PN+SC79 groups. *D–E*, Serum ALT and AST levels in mice from the Ad-PP2A-PN and Ad-PP2A-PN+SC79 groups. *F*, Western blot analyses and densitometric quantification of various proteins of interest. The results are expressed as the mean ± standard deviation (n = 7). $^{*}P < .05$; $^{**}P < .01$.

down-regulated in patients with PNAHS and that hepatic *Ppp2ca* expression was down-regulated in PN mice. The phosphoproteomic data revealed that patients with PNAHS had increased phosphorylation of Akt2 (a PP2A substrate) and decreased phosphorylation of AMPK (PRKAG2). Additionally, PN was associated with the differential expressions of proteins involved in peroxisome function, fatty acid degradation, and PPAR-dependent and AMPK-dependent signaling. Because AMPK is a key regulator of fatty acid β-oxidation[42] and Akt2 inhibits AMPK,[43] our findings provide new evidence that PNAHS involves a down-regulation of PP2A-Cα that activates Akt2 and thereby inhibits AMPK. Notably, experiments demonstrated that PP2A-Cα overexpression protected against PNAHS in mice.

Fatty acid β-oxidation occurs in mitochondria and peroxisomes. Peroxisome loss leads to altered bile acid synthesis and impaired oxidation of VLCFAs, which can induce hepatic steatosis in the setting of malnutrition.[44] However, the effect of fatty acid metabolism on PNAHS is not well-clarified. This study revealed that the differentially expressed proteins were most enriched in peroxisome and fatty acid degradation. Additionally, the animal experiments showed that PNAHS was associated with elevated hepatic ATP level, reduced AMPK phosphorylation at Thr-172 (ie, decreased AMPK activity) and decreased phosphorylation of ACC1 at Ser-79 (ie, enhanced ACC activity). This latter effect would increase the available pool of malonyl CoA for lipid synthesis and reduce fatty acid uptake into mitochondria for β-oxidation. Additionally, hepatic expression of fatty acid β-oxidation genes such as CPT-1 and acetyl-CoA acetyltransferase were reduced in WT-PN and Ppp2ca-LKO-PN mice. The above observations indicate that long-term PN induces downregulation of PP2A-Cα protein expression, which stimulates Akt2 to inhibit AMPK by blocking upstream kinases from phosphorylating it at Thr-172.[45] These alterations cause an elevation of ATP level[46] that reduces fatty acid oxidation.

PNALD is characterized by early cholestasis that sequentially progresses to steatosis, fibrosis, and severe

cirrhosis.[47] Disrupted hepatic cholesterol homeostasis contributes to the pathogenesis of nonalcoholic steatohepatitis and dyslipidemia.[48] Our proteomic results indicated that the differentially expressed proteins were enriched in bile secretion and cholesterol metabolism (Figure 2, *F*), and the differentially phosphorylated proteins could be assigned to

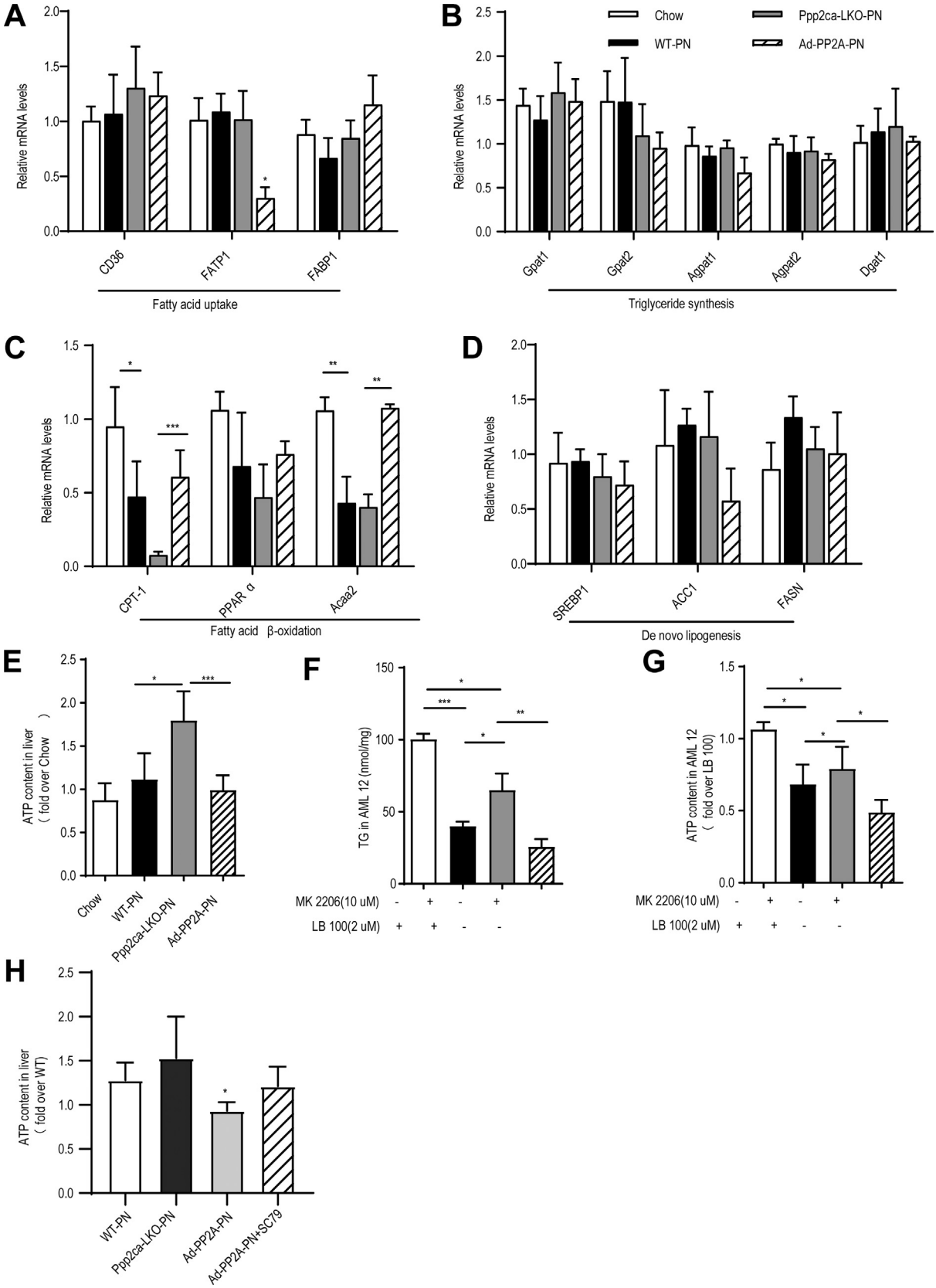

primary bile acid biosynthesis (Figure 2, *L*). Furthermore, cholesterol 7a-hydroxylase (*CYP7A1*; fold-change = 3.08) and sterol 12a-hydroxylase (*CYP8B1*; fold-change = 1.52), which is the rate-limiting enzyme in the conversion of cholesterol to primary bile acids, were strongly up-regulated in patients with PNAHS (Supplementary Data 1). A previous study reported that up-regulation of CYP7A1 and CYP8B1 and enhanced synthesis of hepatotoxic bile acids contribute to short bowel syndrome-associated liver disease.[35] These mechanisms may also be involved in the pathogenesis of cholestasis and hepatic steatosis following PN.

Published data regarding the progression of PNAHS are limited.[49,50] Most previous studies have focused on PN-associated cholestasis and inflammation,[5,8,9,51,52] and the previous animal models used have mainly included neonatal piglets, dogs, rats and mice.[5,50,53] The murine model is a key platform for mechanistic and therapeutic studies, and they provide the option of genetic manipulation.[54] Therefore, we developed a mice model of PN. When compared with chow mice, animals receiving PN developed mild hepatic steatosis after 7 days, as described previously,[49] and more severe hepatic steatosis after 14 or 28 days. Because mortality increased with prolonged duration of PN, most of our experiments used a PN duration of 14 days, which achieved a good balance between the degree of hepatic steatosis and survival rate. Our mice model could be used to facilitate studies of PNAHS that aim at exploring mechanisms and potential novel therapies.

Previous study indicated SAMe prevents PN-induced cholestasis[55,56] and fatty liver disease.[37,57,58] SAMe is a critical regulator of PP2A activity,[37] which upregulates PP2A expression[59] and methylates the catalytic subunit of PP2A.[60,61] We found that liver content in SAMe was decreased as a consequence of PN. This will explain why the expression of PP2ACα was downregulated in the human and mice PNAHS model.

However, our study has some limitations. Intervention trials of PP2A in humans have not been performed because PP2A activators or effector analogs were unavailable for clinical use. Further clinical studies are warranted to investigate the effects of PP2A intervention on the development of hepatic steatosis in patients receiving long-term PN.

In conclusion, our findings suggest that PNAHS involves the downregulation of hepatic PP2ACα and consequent activation of Akt2, which in turn inhibits AMPK to alter hepatic lipid metabolism and promote TG accumulation and liver injury. Our study provides a strong rationale that PP2A-Cα may be involved in the pathogenesis of PNAHS. Further research is merited to establish whether interventions to enhance PP2A function might suppress the development of hepatic steatosis in patients receiving long-term PN.

Materials and Methods

Human Samples

Human liver specimens were obtained from 10 patients with PNAHS[62] and 8 cholelithiasis (controls) patients admitted to the Department of General Surgery, Jinling Hospital, Medical School of Nanjing University from June 2018 to June 2019.

Inclusion criteria: age ≥18 years, receiving PN for IF (short bowel syndrome, type II or type III) from June 2018 to June 2019, duration of PN >6 months, and diagnosed with PNALD-steatosis by AAR index or liver ultrasound echogenic.[63] AAR index: AST/ALT ratio <1 when AST and ALT > upper limit of normal. All 18 patients included in the study exhibited no evidence of other liver diseases (including viral hepatitis, alcoholic/non-alcoholic liver disease, biliary atresia, primary biliary cholangitis, Wilson's disease, alpha-1 antitrypsin deficiency, or other inherited liver diseases) or metabolic diseases (including diabetes mellitus, hyperthyroidism, or insulin resistance) based on standard clinical, laboratory, and histological assessments. The clinical characteristics of the study participants were collected from the electronic database and are detailed in Table 1, Supplementary Table 4, and Supplementary Table 5. Liver biopsies were obtained from patients with PNALD-steatosis by experienced radiologists under ultrasound guidance or during a planned laparotomy. Liver fat content was assessed by computed tomography, and staining of liver samples with oil red O. All participants provided informed consent for inclusion in the study, which was approved by the Ethics Committee of Jinling Hospital (2017NZGKJ-071).

Proteomic/Phosphoproteomic Analyses

Sample preparation. Liver tissue was ground under liquid nitrogen and re-suspended in lysis buffer containing 7 M urea, 30 mM 4-(2-hydroxyethyl)-1-piperazineethanesulfonic acid, 2 mM ethylenediaminetetraacetic acid, 10 mM dithiothreitol (DTT), 4% sodium dodecyl sulfate (SDS), 1 mM phenylmethylsulfonyl fluoride, and 1X protease inhibitor. The lysate was sonicated (2 × 15 seconds, 180 W) on ice and centrifuged at 10,000 × g for 30 minutes at 4 ºC. The cleared lysate was placed in a clean tube, and the concentration was normalized. Protein cysteine residues were then reduced with DTT for 60 min at 55 ºC, alkylated with 35 mM iodoacetamide for 60 minutes at room temperature in the dark, and quenched with an additional 10 mM DTT for 15 minutes at room temperature. Volumes of acetone (4×, −20°C) were added to precipitate the protein overnight. Precipitated protein was collected via

Figure 10. (***See previous page***). **Representative mRNA expression and ATP content in mice.** *A–D*, mRNA expression of fatty acid uptake, triglyceride synthesis, do novo lipogenesis, and fatty acid β-oxidation genes in the liver tissues from mice in the chow (14 days), WT-PN (14 days), Ppp2ca-LKO-PN (14 days), and Ad-PP2A-PN (14 days) groups. *E*, Hepatic adenosine triphosphate (ATP) content for mice in the chow (14 days), WT-PN (14 days), Ppp2ca-LKO-PN (14 days), and Ad-PP2A-PN (14 days) groups. *F–G*, TG and ATP content of AML12 cells. Some AML12 cells were treated with 2 μM LB-100 (a PP2A inhibitor) or/and 10 μM MK-2206 (an Akt inhibitor) for 24 hours. *H*, Hepatic ATP content for mice in the WT-PN (14 days), Ad-PP2A-PN (14 days), and Ad-PP2A+SC79 (14 days) groups. The results are expressed as the mean ± standard deviation (n = 5–7). **P* < .05; ***P* < .01; ****P* < .001.

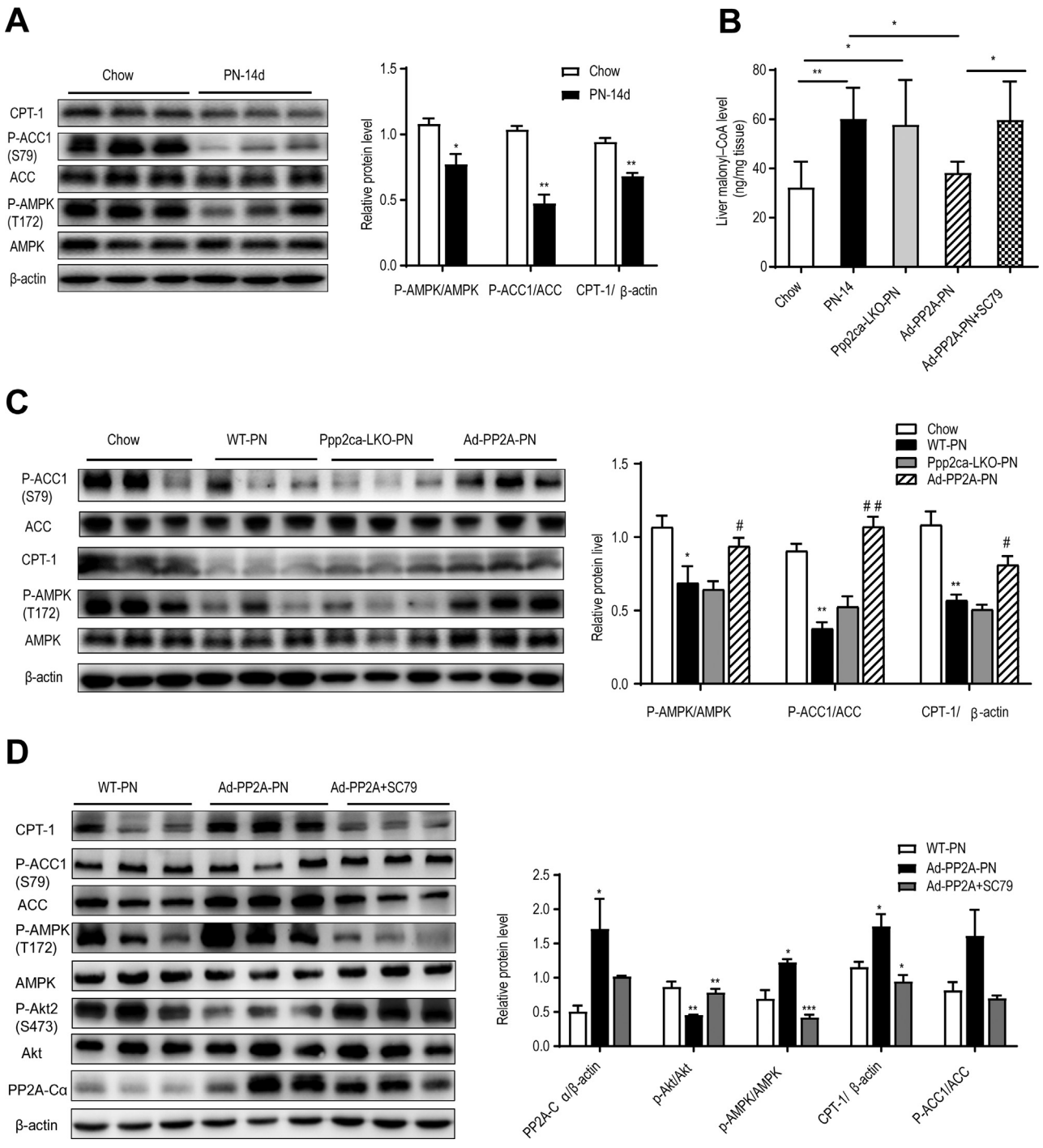

Figure 11. PP2A-Cα regulates fatty acid β-oxidation in an Akt2-adenosine AMPK-dependent manner in mice given PN. *A, C–D*, Representative Western blots and densitometric quantification of the protein of phosphorylated acetyl-CoA carboxylase (p-ACC, Ser-79), CPT-1, phosphorylated AMPK (p-AMPK, Thr-172), phosphorylated Akt (p-Akt, Ser-473), and catalytic subunit of protein phosphatase-2A (PP2A-Cα) in liver tissues from mice. *B*, Hepatic concentrations of malonyl-CoA in the 4 (chow, WT-PN, Ppp2ca-LKO-PN, and Ad-PP2A-PN) groups of mice. The results are expressed as the mean ± standard deviation (n = 5–7). **P* < .05; ***P* < .01; ***P < .001.

centrifugation at 2000 × g for 20 minutes at 4°C. The pellet was resuspended in 0.1 mL of an acetone-ethanol mixture (1:1), allowed to stand at −20 °C for 3 hours, and then centrifuged at 20000 × g at 4 °C for 30 minutes. The supernatant was discarded, the pellet was resuspended in acetone-ethanol mixture, and the above steps were repeated twice. Finally, 110 μL of 100 mM triethylammonium bicarbonate solution was added.

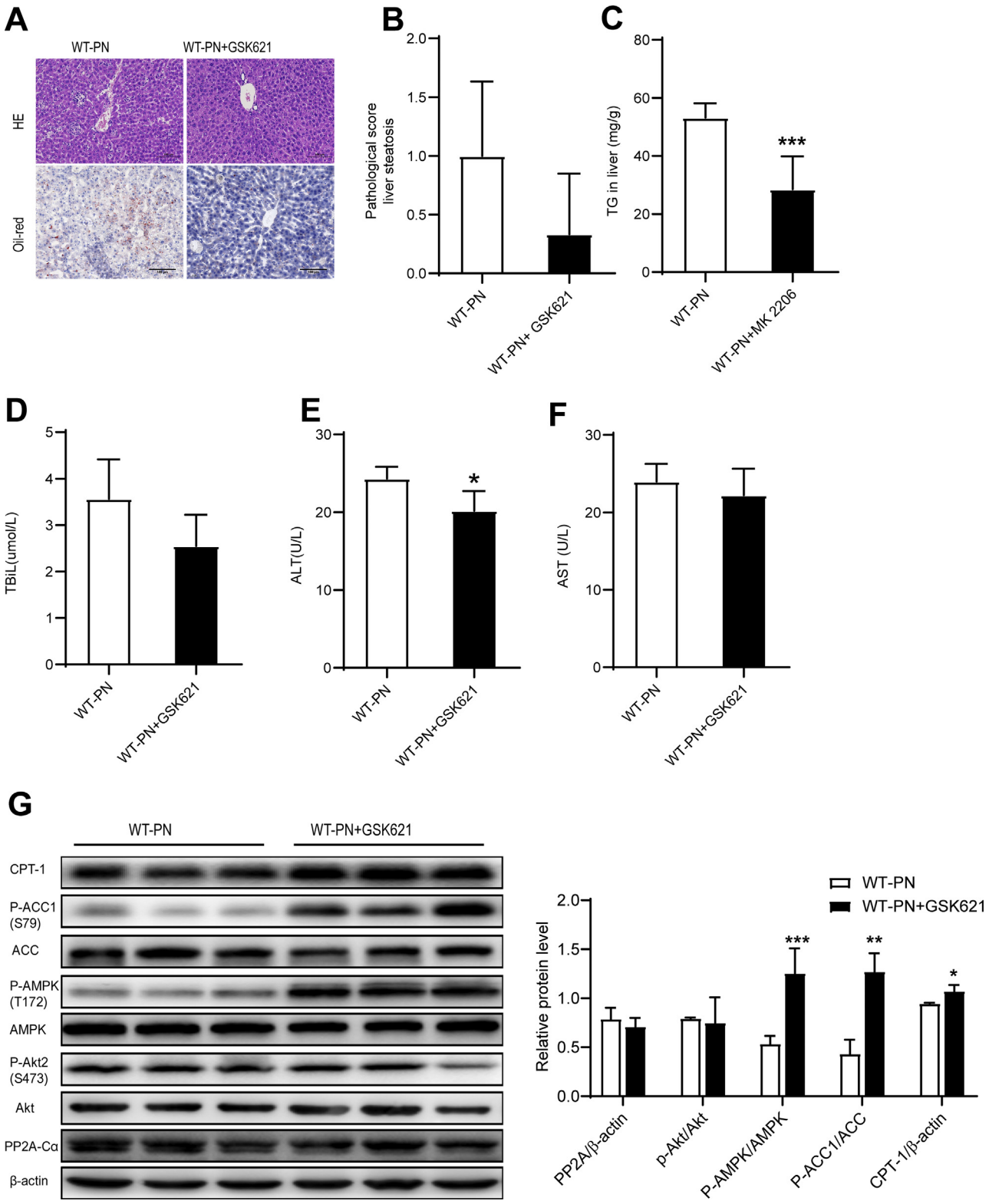

Figure 12. AMPK hyperactivation alleviated PNAHS in mice. *A*, Representative images showing liver sections stained with HE or oil red O from mice in the WT-PN group and WT-PN+GSK621 group (mice treated with GSK621, an activator of AMPK). *B*, Pathological scores for hepatic steatosis determined from oil red O sections in a blinded manner. *C*, TG levels in liver homogenates from mice in the WT-PN group and WT-PN+GSK621 group. *D–F*, Serum TBIL, ALT, and AST levels in mice from the WT-PN group and WT-PN+GSK621. *G*, Western blot analyses and densitometric quantification of various proteins of interest. The results are expressed as the mean ± standard deviation (n = 7). **P* < .05; ***P* < .01; ****P* < .001.

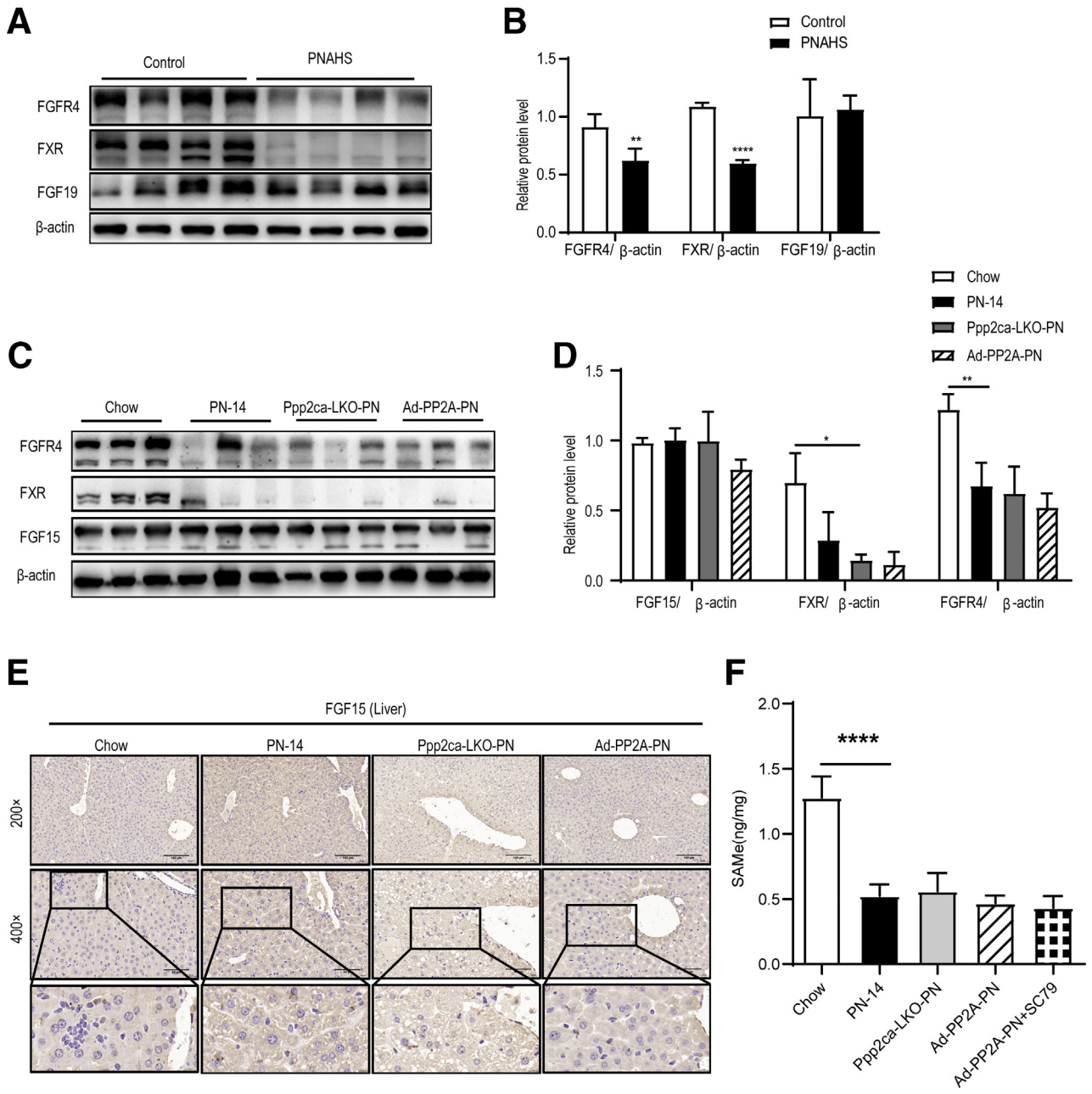

Figure 13. FGF15/19 signaling pathway associated protein abundances in patients and mice. *A–B*, Representative Western blots and densitometric quantification of the proteins of FGF19, FXR, and FGFR4 in liver tissues from patients with PNAHS and controls. *C–D*, Representative Western blots and densitometric quantification of the proteins of FGF15, FXR, and FGFR4 in liver tissues from mice in the chow (14 days), WT-PN (14 days), Ppp2ca-LKO-PN (14 days), and Ad-PP2A-PN (14 days) groups. *E*, Representative immunohistochemical images of FGF15 protein distribution in liver from mice in the chow (14 days), WT-PN (14 days), Ppp2ca-LKO-PN (14 days), and Ad-PP2A-PN (14 days) groups. *F*, Quantification of liver SAMe concentration in mice liver. The results are expressed as the mean ± standard deviation (n = 5–7). **P* < .05; ***P* < .01; ****P* < .001; *****P* < .0001.

Trypsin Digestion and Phosphopeptide Enrichment

On-filter digestion of the protein with trypsin was performed overnight in a wet chamber at 37 °C using a trypsin-to-protein ratio of 1:100 (w/w). After digestion, the samples were acidified with trifluoroacetic acid to pH 2 and desalted using a SepPack column in accordance with the manufacturer's instructions (C18 cartridges, Sep-Pak Vac, 1 cc [50 mg]; Waters Corp, Eschborn, Germany). Eluates were dried and stored at −80 °C. Tandem mass tag (TMT) labeling was performed in accordance with the manufacturer's instructions (TMT10plex Isobaric Label Reagent Set; Thermo Fisher Scientific, Bremen, Germany). Briefly, samples were resolved in 40 μL of 50-mM

triethylammonium bicarbonate solution (1.0 M, pH 8.5; Sigma Aldrich, St. Louis, MO). For each sample, 60 μL of TMT stock solution was added to 300 μg of digested protein. Ten TMT-labeled samples were combined for phosphopeptide enrichment, which was performed using an analytical Fe-IMAC column (4 × 50 mm ProPac IMAC-10; Thermo Fisher Scientific) connected to a high-performance liquid chromatography system (AEKTA Explorer FPLC system; Amersham Pharmacia, Amersham, United Kingdom). The phosphopeptide fraction and flow-through were collected according to the ultraviolet signal (280 nm), dried down and stored at −80 °C.

Nanoscale Liquid Chromatography Coupled to Tandem Mass Spectrometry (Nano-LC-MS/MS)

For each sample, 1 μg of total peptides were separated and analyzed with a nano-ultra-performance liquid chromatography system (EASY-nLCTM 1200; Thermo Fisher Scientific) coupled to a mass spectrometer (Q Exactive HF-X Orbitrap instrument; Thermo Fisher Scientific) with a nano-electrospray ion source. Separation was performed using a reversed-phase column (Reprosil-Pur 120 C18-AQ, 100 μm internal diameter × 15 cm, 1.9 μm particle size; Dr Maisch, Ammerbuch, Germany). The mobile phases were H2O containing 0.1% formic acid and 2% acetonitrile (phase A) or 80% acetonitrile and 0.1% formic acid (phase B). Separation of the sample was carried out at a flow rate of 300 nL/min using the following gradients: 2% to 5% B for 2 minutes, 5% to 22% B for 68 minutes, 22% to 45% B for 16 minutes, 45% to 95% B for 2 minutes, and 95% B for 2 minutes.

Data-dependent acquisition was performed in profile and positive modes with an Orbitrap analyzer at a resolution of 120,000 (@ m/z 200) and an m/z range of 350 to 1600 for MS1. For MS2, the resolution was set to 45,000 with a fixed first mass of 110 m/z. The automatic gain control (AGC) target was set to 3 × 106 with a maximum injection time of 30 ms for MS1 and 1 × 105 with a maximum injection time of 96 ms for MS2. The top 20 most intense ions were fragmented by high-energy collisional dissociation with a normalized collision energy of 32% and an isolation window of 0.7 m/z. The dynamic exclusion time window was 45 seconds. Single-charged peaks and peaks with a charge exceeding 6 were excluded from the data-dependent acquisition procedure.

Nano-LC-MS/MS Data Acquisition for Phosphoproteomic

Each fraction was resuspended in 6 μL solvent A (water with 0.1% formic acid), separated by nano-LC and analyzed by online electrospray tandem mass spectrometry. The experiments were performed on an EASY-nLCTM 1200 system (Thermo Fisher Scientific) connected to a mass spectrometer (Orbitrap Exploris 480; Thermo Fisher Scientific) equipped with an online nano-electrospray ion source. A 3-μL peptide sample was loaded onto the analytical column and subsequently separated with a linear gradient from 1% solvent B (acetonitrile with 0.1% formic acid) to 28% solvent B for 130 minutes, 28% solvent B to 60% solvent B for 13 minutes, and 60% solvent B to 100% solvent B for 1 minutes, and the sample was held there for 6 minutes. The column flow rate was maintained at 300 nL/min, and the electrospray voltage relative to the inlet of the mass spectrometer was 2.3 kV.

The Orbitrap Exploris 480 mass spectrometer was operated in the data-dependent mode to switch automatically between MS and MS/MS acquisition. Survey full-scan MS spectra (m/z 400–1600) were acquired with a mass resolution of 120,000. The AGC target was set to 1 × 106, and the maximum injection time was 50 ms. Ten sequential high-energy collisional dissociation MS/MS scans with a resolution of 30,000 were acquired, with an intensity threshold of 50,000 and a maximum injection time of 60 ms. The AGC target was set to 1.0 × 105, and the isolation window was 1.6 m/z. Ions with charge states 2+, 3+, and 4+ were fragmented with a normalized collision energy of 35%. In all cases, one microscan was recorded using a dynamic exclusion of 10 seconds.

Database Searching for Phosphoproteomic Analyses

Tandem mass spectra were extracted using Proteome Discoverer version 2.4.0.305 (Thermo Fisher Scientific). All MS/MS samples were analyzed using Sequest software, which was set up to search the Uniprot database (Homo sapiens, 2020-03-10; 20,366 reviewed entries) with carbamidomethyl (C), TMT 6 plex (K), and TMT 6 plex (N-term) as a fixed modification and oxidation (M) and phosphorylation (S, T, Y) as variable modifications. Trypsin was used as the protease. Sequest was searched with a fragment ion mass tolerance of 20 mmu and a parent ion tolerance of 10 ppm. A maximum of 2 missed cleavages was allowed. The percolator algorithm was used to keep the peptide-spectrum matches-level and peptide-level false discovery rates below 1%.

Database Searching Using Proteome Discoverer

The raw MS files were processed using Proteome Discoverer version 2.4.0.305 (Thermo Fisher Scientific) and the built-in Sequest HT search engine. MS spectra lists were searched against their species-level UniProt FASTA databases (uniprot-Human-9606-2020-10. fasta), with carbamidomethyl (C), TMT 6 plex (K), and TMT 6 plex (N-term) as fixed modifications and oxidation (M) and acetylation (N-terminal) as variable modifications. Trypsin was used as the protease. A maximum of 2 missed cleavages was allowed. The false discovery rate was set to 0.01 for both the peptide-spectrum matches and peptide levels. Peptide identification was performed with an initial precursor mass deviation of up to 10 ppm and a fragment mass deviation of 0.02 Da. Unique peptides and razor peptides were used for protein quantification, and the total peptide amount was used for normalization. All the other parameters were reserved as default.

Animal Experiments

Animals. WT C57BL/6J male mice aged 8 to 10 weeks old and liver-specific PP2A-Cα-knockout (Ppp2ca-LKO) male mice on a C57BL/6J background (Model Animal Research

Center of Nanjing University, Nanjing, China) were maintained at the animal facility of Nanjing University Medical School. All mice were maintained under specific pathogen-free conditions at the animal facility of Nanjing University Medical School.

The animals were housed in a 12-hour light/dark cycle at 25 °C ± 2 °C with free access to rodent chow and water. The animal studies were approved by the Institutional Animal Care and Use Committee of Jinling Hospital, Medical School of Nanjing University.

Design of the animal experiments. Mice were administered 2.5% DSS (MP Biomedicals, Santa Ana, CA) for 4 days to induce mild intestinal injury (the animals also had access to chow ad libitum). After pretreatment with DSS, the mice were anesthetized by intraperitoneal administration of 5 mg/kg carprofen. For mice receiving PN, a central venous catheter (silastic tubing with an internal diameter of 0.012 inches; Dow Corning, Midland, MI) was surgically placed into the right jugular vein, and the proximal end was tunneled subcutaneously to exit between the shoulder blades. Mice were recovered from anesthesia on a heating pad under continuous supervision and allowed to further recover from surgery for 24 hours, during which they were infused with intravenous normal saline at a rate of 0.23 mL/h and given ad libitum access to chow and water (the mice were partially restrained by the tail to protect the catheter during infusion).

After recovery, mice in the chow group (n = 7) received a diet of standard laboratory chow and water as well as continuous infusion of normal saline (0.4 mL/h), whereas mice in the PN group received continuous infusion of PN solution (0.4 mL/h) without access to chow. Body weight was recorded every 2 days. After receiving enteral feeding or PN for 7 days (n = 7), 14 days (n = 7), or 28 days (n = 5), the mouse was anesthetized and its body weight recorded. To inhibit Akt-dependent signaling, the mice were gavaged with MK-2206 (360 mg/kg/week; #A3010, Apexbio, Boston, MA).[64] To activate Akt-dependent signaling, mice were administered SC79[65] by intraperitoneal injection (20 mg/kg/week; #B5663, Apexbio). To activate AMPK-dependent signaling, the mice were given GSK621 (#B6020, Apexbio).[66] by intraperitoneal injection (30 mg/kg/day).

Blood was collected from the retro-orbital plexus, and serum was prepared by centrifugation (3000 rpm, 10 minutes) and stored at −80 ℃ for later analysis. The entire liver, epididymal fat, and quadriceps were rapidly excised and weighed. A random biopsy was then taken from the liver and fixed overnight in 4% formalin for histological analysis. The remaining liver samples were immediately frozen in liquid nitrogen.

Generation and Use of Recombinant Adenoviruses

The plasmid was constructed by WZ Biosciences Inc (Columbia, MD). Adenoviruses expressing full-length mouse Ppp2ca (Ad-Ppp2ca, n = 8) and control adenoviruses expressing green fluorescent protein (Ad-GFP, n = 7) were prepared. All viruses were purified by the cesium chloride method and dialyzed in phosphate-buffered saline containing 10% glycerol prior to injection into animals. Adenoviruses (1 × 109 plaque-forming units) were injected into the mice via the central vein.

Cell Lines

AML12 cells (mouse liver cells) were provided by Professor Chaojun Li (Nanjing University Medical School). AML12 cells were cultured in Dulbecco's Modified Eagle Medium: F-12 containing 10% fetal bovine serum (Gibco, Carlsbad, CA). The cells were treated with the PP2A inhibitor LB-100 (2 μM; #B4846, Apexbio), the AKT inhibitor MK-2206 (10 μM; #A3010, Apexbio) or the Akt agonist SC79 (5 μg/mL; #B5663, Apexbio) for 24 hours.

Biochemistry

Plasma AST (Cat#: C010-2), ALT (Cat#: C009-2), alkaline phosphatase (Cat#: A059-2), free fatty acid (Cat#: A042-2), TBIL (Cat#: C019-1), total cholesterol (Cat#: A111-1), high-density lipoprotein cholesterol (Cat#: A112-1), low-density lipoprotein cholesterol (Cat#: A113-1), TG (Cat#: A110-1), and albumin (Cat#: A028-2) were measured using commercially available detection kits (Nanjing Jiancheng Bioengineering Institute, Nanjing, China).

Liver tissue was homogenized in absolute alcohol. Liver TG was assayed using a commercial kit (A110-2-1, Nanjing Jiancheng Bioengineering Institute) in accordance with the manufacturer's protocol. Liver TG levels are expressed as nmol/mg protein. ATP concentrations in liver tissue samples (at least 25 mg) were measured with an ATP Content Assay Kit (BC0305, Solarbio, Beijing, China). AML12 cells were plated in 6-well plates at the start of the experiment. After treatment, the cells were subjected to ultrasonic disruption and then centrifuged at 800 × g for 10 minutes at 4ºC, and the supernatant was collected for detection. SAMe concentrations in liver tissue samples were detected using the enzyme-linked immunosorbent assay kit (RF5535; Shanghai Ruifan Biotechnology, Shanghai, China). Hepatic concentrations of malonyl-CoA were measured by enzyme-linked immunosorbent assay (CSB-E12896m; Cusabio, China).

Histology

The liver tissue was fixed in 4% paraformaldehyde (pH 7.4), embedded in paraffin and sectioned (5 μm). The sections were stained with HE for morphological examination and Sirius Red or Masson's trichrome for fibrosis staining. Lipid droplets in liver cryosections (7 μm) were stained with oil red O using a commercially available kit (Wuhan Service Biotechnology, Wuhan, China). Immunohistochemical staining was performed with FGF15 antibody. Pathological scores for steatosis were calculated using protocols described previously.[67] The degree of liver fibrosis was also estimated using the APRI and the Fibrosis-4 index based on patient age, AST, ALT, and platelet count.

RNA Isolation and Real-time Polymerase Chain Reaction (PCR)

Total RNA was isolated from liver tissue using TRIzol reagent (Invitrogen, Carlsbad, CA). Reverse transcription

was performed using a Prime Script II 1st Strand cDNA Synthesis Kit (Takara Bio, Inc, Tokyo, Japan) in accordance with the manufacturer's instructions. The mRNA expression levels were determined using real-time PCR Master Mix (Toyobo, Osaka, Japan) and a ViiATM 7 Real-time PCR System (Applied Biosystems, Foster City, CA). β-actin was used as an internal control to calculate relative mRNA expression. The primers used for gene amplification are detailed in Supplementary Table 2.

Immunoblotting

Liver tissue was homogenized in RIPA Lysis Buffer (50 mM Tris [pH 7.4], 150 mM NaCl, 1% Triton X-100, 1% sodium deoxycholate, 0.1% SDS, sodium orthovanadate, sodium fluoride, ethylenediaminetetraacetic acid, and leupeptin). The homogenate was incubated for 40 minutes on ice and then centrifuged at 12,000 $\times$ g for 10 minutes at 4 °C. Supernatants were collected, and the protein concentration was measured using a bicinchoninic acid assay kit (23227; Thermo Fisher Scientific). Equal amounts of protein (30 μg) from each sample were resolved on 10% to 16% SDS-PAGE gels, transferred onto polyvinylidene fluoride membranes, and blotted with appropriate antibodies. All immunoblotting experiments were repeated more than 3 times. The primary antibodies used are listed in Supplementary Table 3.

Statistical Analysis

No statistical methods were used to predetermine the sample size. The analysis was performed using Prism 8 for Windows (GraphPad Software, La Jolla, CA). Data are expressed as the mean $\pm$ standard deviation of at least 3 independent experiments. For data that passed normality tests, the Student t test was used when differences between 2 groups were analyzed, and analysis of variance was used when differences between 3 or more groups were compared. For the differential proteins and phosphorylation sites, the significance level was set at P-value $< .05$, fold change < 0.77, or fold change > 1.3. $P < .05$ was considered significant.

References

1. Pironi L, Arends J, Bozzetti F, Cuerda C, Gillanders L, Jeppesen PB, Joly F, Kelly D, Lal S, Staun M, Szczepanek K, Van Gossum A, Wanten G, Schneider SM. Home Artificial Nutrition and Chronic Intestinal Failure Special Interest Group of ESPEN. ESPEN guidelines on chronic intestinal failure in adults. Clin Nutr 2016;35:247–307.
2. Doig GS, Simpson F, Sweetman EA, Finfer SR, Cooper DJ, Heighes PT, Davies AR, O'Leary M, Solano T, Peake S. Early PN Investigators of the ANZICS Clinical Trials Group. Early parenteral nutrition in critically ill patients with short-term relative contraindications to early enteral nutrition: a randomized controlled trial. JAMA 2013;309:2130–2138.
3. Mutanen A, Lohi J, Heikkilä P, Koivusalo AI, Rintala RJ, Pakarinen MP. Persistent abnormal liver fibrosis after weaning off parenteral nutrition in pediatric intestinal failure. Hepatology 2013;58:729–738.
4. Lauriti G, Zani A, Aufieri R, Cananzi M, Chiesa PL, Eaton S, Pierro A. Incidence, prevention, and treatment of parenteral nutrition-associated cholestasis and intestinal failure-associated liver disease in infants and children: a systematic review. JPEN J Parenter Enteral Nutr 2014;38:70–85.
5. El Kasmi KC, Anderson AL, Devereaux MW, Fillon SA, Harris JK, Lovell MA, Finegold MJ, Sokol RJ. Toll-like receptor 4-dependent Kupffer cell activation and liver injury in a novel mouse model of parenteral nutrition and intestinal injury. Hepatology 2012;55:1518–1528.
6. Mutanen A, Lohi J, Heikkilä P, Jalanko H, Pakarinen MP. Loss of ileum decreases serum fibroblast growth factor 19 in relation to liver inflammation and fibrosis in pediatric onset intestinal failure. J Hepatol 2015;62:1391–1397.
7. Mutanen A, Lohi J, Sorsa T, Jalanko H, Pakarinen MP. Features of liver tissue remodeling in intestinal failure during and after weaning off parenteral nutrition. Surgery 2016;160:632–642.
8. El Kasmi KC, Vue PM, Anderson AL, Devereaux MW, Ghosh S, Balasubramaniyan N, Fillon SA, Dahrenmoeller C, Allawzi A, Woods C, McKenna S, Wright CJ, Johnson L, D'Alessandro A, Reisz JA, Nozik-Grayck E, Suchy FJ, Sokol RJ. Macrophage-derived IL-1β/NF-κB signaling mediates parenteral nutrition-associated cholestasis. Nat Commun 2018;9:1393.
9. Mutanen A, Lohi J, Heikkilä P, Jalanko H, Pakarinen MP. Liver inflammation relates to decreased canalicular bile transporter expression in pediatric onset intestinal failure. Ann Surg 2018;268:332–339.
10. Whiteman EL, Cho H, Birnbaum MJ. Role of Akt/protein kinase B in metabolism. Trends Endocrinol Metab 2002;13:444–451.
11. Jeong SH, Kim HB, Kim MC, Lee JM, Lee JH, Kim JH, Kim JW, Park WY, Kim SY, Kim JB, Kim H, Kim JM, Choi HS, Lim DS. Hippo-mediated suppression of IRS2/AKT signaling prevents hepatic steatosis and liver cancer. J Clin Invest 2018;128:1010–1025.
12. He L, Hou X, Kanel G, Zeng N, Galicia V, Wang Y, Yang J, Wu H, Birnbaum MJ, Stiles BL. The critical role of AKT2 in hepatic steatosis induced by PTEN loss. Am J Pathol 2010;176:2302–2308.
13. Cho H, Mu J, Kim JK, Thorvaldsen JL, Chu Q, Crenshaw EB 3rd, Kaestner KH, Bartolomei MS, Shulman GI, Birnbaum MJ. Insulin resistance and a diabetes mellitus-like syndrome in mice lacking the protein kinase Akt2 (PKB beta). Science 2001;292:1728–1731.
14. Jeon SM. Regulation and function of AMPK in physiology and diseases. Exp Mol Med 2016;48:e245.
15. Garcia D, Hellberg K, Chaix A, Wallace M, Herzig S, Badur MG, Lin T, Shokhirev MN, Pinto AFM, Ross DS, Saghatelian A, Panda S, Dow LE, Metallo CM, Shaw RJ. Genetic liver-specific AMPK activation protects against diet-induced obesity and NAFLD. Cell Rep 2019;26:192–208.e6.

16. Liou CJ, Lee YK, Ting NC, Chen YL, Shen SC, Wu SJ, Huang WC. Protective effects of licochalcone A ameliorates obesity and non-alcoholic fatty liver disease via promotion of the Sirt-1/AMPK pathway in mice fed a high-fat diet. Cells 2019;8:447.
17. Woods A, Williams JR, Muckett PJ, Mayer FV, Liljevald M, Bohlooly YM, Carling D. Liver-specific activation of AMPK prevents steatosis on a high-fructose diet. Cell Rep 2017;18:3043–3051.
18. Andjelković M, Jakubowicz, Cron FX, Ming WJ, Han AB, Hemmings. Activation and phosphorylation of a pleckstrin homology domain containing protein kinase (RAC-PK/PKB) promoted by serum and protein phosphatase inhibitors. Proc Natl Acad Sci U S A 1996;93:5699–5704.
19. Mistafa O, Ghalali A, Kadekar S, Hogberg J, Stenius U. Purinergic receptor-mediated rapid depletion of nuclear phosphorylated Akt depends on pleckstrin homology domain leucine-rich repeat phosphatase, calcineurin, protein phosphatase 2A, and PTEN phosphatases. J Biol Chem 2010;285:27900–27910.
20. Janssens V, Goris J. Protein phosphatase 2A: a highly regulated family of serine/threonine phosphatases implicated in cell growth and signalling. Biochem J 2001; 353(Pt 3):417–439.
21. Sontag E. Protein phosphatase 2A: the Trojan Horse of cellular signaling. Cell Signal 2001;13:7–16.
22. Janssens V, Longin S, Goris J. PP2A holoenzyme assembly: in cauda venenum (the sting is in the tail). Trends Biochem Sci 2008;33:113–121.
23. Khew-Goodall Y, Hemmings BA. Tissue-specific expression of mRNAs encoding alpha- and beta-catalytic subunits of protein phosphatase 2A. FEBS Lett 1988;238:265–268.
24. Albadrani M, Seth RK, Sarkar S, Kimono D, Mondal A, Bose D, Porter DE, Scott GI, Brooks B, Raychoudhury S, Nagarkatti M, Nagarkatti P, Jule Y, Diehl AM, Chatterjee S. Exogenous PP2A inhibitor exacerbates the progression of nonalcoholic fatty liver disease via NOX2-dependent activation of miR21. Am J Physiol Gastrointest Liver Physiol 2019;317:G408–G428.
25. Van Kanegan MJ, Adams DG, Wadzinski BE, Strack S. Distinct protein phosphatase 2A heterotrimers modulate growth factor signaling to extracellular signal-regulated kinases and Akt. J Biol Chem 2005;280:36029–36036.
26. Jo H, Mondal S, Tan D, Nagata E, Takizawa S, Sharma AK, Hou Q, Shanmugasundaram K, Prasad A, Tung JK, Tejeda AO, Man H, Rigby AC, Luo HR. Small molecule-induced cytosolic activation of protein kinase Akt rescues ischemia-elicited neuronal death. Proc Natl Acad Sci U S A 2012;109:10581–10586.
27. Hahn-Windgassen A, Nogueira V, Chen CC, Skeen JE, Sonenberg N, Hay N. Akt activates the mammalian target of rapamycin by regulating cellular ATP level and AMPK activity. J Biol Chem 2005;280:32081–32089.
28. Nishimura T, Utsunomiya Y, Hoshikawa M, Ohuchi H, Itoh N. Structure and expression of a novel human FGF, FGF-19, expressed in the fetal brain. Biochim Biophys Acta 1999;18:148–151.
29. Fon Tacer K, Bookout AL, Ding X, Kurosu H, John GB, Wang L, Goetz R, Mohammadi M, Kuro-o M, Mangelsdorf DJ, Kliewer SA. Research resource: comprehensive expression atlas of the fibroblast growth factor system in adult mouse. Mol Endocrinol 2010; 24:2050–2064.
30. Gadaleta RM, Moschetta A. Metabolic Messengers: fibroblast growth factor 15/19. Nat Metab 2019;1:588–594.
31. Khambu B, Li T, Yan S, Yu C, Chen X, Goheen M, Li Y, Lin J, Cummings OW, Lee YA, Friedman S, Dong Z, Feng GS, Wu S, Yin XM. Hepatic autophagy deficiency compromises farnesoid X receptor functionality and causes cholestatic injury. Hepatology 2019;69:2196–2213.
32. Potthoff MJ, Kliewer SA, Mangelsdorf DJ. Endocrine fibroblast growth factors 15/19 and 21: from feast to famine. Genes Dev 2012;26:312–324.
33. Alvarez-Sola G, Uriarte I, Latasa MU, Fernandez-Barrena MG, Urtasun R, Elizalde M, Barcena-Varela M, Jimenez M, Chang HC, Barbero R, Catalan V, Rodriguez A, Fruhbeck G, Gallego-Escuredo JM, Gavalda-Navarro A, Villarroya F, Rodriguez-Ortigosa CM, Corrales FJ, Prieto J, Berraondo P, Berasain C, Avila MA. Fibroblast growth factor 15/19 (FGF15/19) protects from diet-induced hepatic steatosis: development of an FGF19-based chimeric molecule to promote fatty liver regeneration. Gut 2017;66:1818–1828.
34. Bhatnagar S, Damron HA, Hillgartner FB. Fibroblast growth factor-19, a novel factor that inhibits hepatic fatty acid synthesis. J Biol Chem 2009;284:10023–10033.
35. Pereira-Fantini PM, Lapthorne S, Joyce SA, Dellios NL, Wilson G, Fouhy F, Thomas SL, Scurr M, Hill C, Gahan CG, Cotter PD, Fuller PJ, Hardikar W, Bines JE. Altered FXR signalling is associated with bile acid dysmetabolism in short bowel syndrome-associated liver disease. J Hepatol 2014;61:1115–1125.
36. El Kasmi KC, Ghosh S, Anderson AL, Devereaux MW, Balasubramaniyan N, D'Alessandro A, Orlicky DJ, Suchy FJ, Shearn CT, Sokol RJ. Pharmacologic activation of hepatic farnesoid X receptor prevents parenteral nutrition associated cholestasis in mice. Hepatology 2022;75:252–265.
37. Zubiete-Franco I, Garcia-Rodriguez JL, Martinez-Una M, Martinez-Lopez N, Woodhoo A, Juan VG, Beraza N, Lage-Medina S, Andrade F, Fernandez ML, Aldamiz-Echevarria L, Fernandez-Ramos D, Falcon-Perez JM, Lopitz-Otsoa F, Fernandez-Tussy P, Barbier-Torres L, Luka Z, Wagner C, Garcia-Monzon C, Lu SC, Aspichueta P, Mato JM, Martinez-Chantar ML, Varela-Rey M. Methionine and S-adenosylmethionine levels are critical regulators of PP2A activity modulating lipophagy during steatosis. J Hepatol 2016;64:409–418.
38. Chen L, Guo P, Li W, Fang F, Zhu W, Fan J, Wang F, Gao Y, Zhao Q, Wang Q, Xiao Y, Xing X, Li D, Shi T, Yu D, Aschner M, Zhang L, Chen W. Perturbation of specific signaling pathways is involved in initiation of mouse liver fibrosis. Hepatology 2021;73:1551–1569.
39. Xian L, Hou S, Huang Z, Tang A, Shi P, Wang Q, Song A, Jiang S, Lin Z, Guo S, Gao X. Liver-specific deletion of Ppp2cα enhances glucose metabolism and insulin sensitivity. Aging (Albany NY) 2015;7:223–232.
40. Chen XY, Cai CZ, Yu ML, Feng ZM, Zhang YW, Liu PH, Zeng H, Yu CH. LB100 ameliorates nonalcoholic fatty

liver disease via the AMPK/Sirt1 pathway. World J Gastroenterol 2019;25:6607–6618.
41. Zhao C, Liu L, Liu Q, Li F, Zhang L, Zhu F, Shao T, Barve S, Chen Y, Li X, McClain CJ, Feng W. Fibroblast growth factor 21 is required for the therapeutic effects of Lactobacillus rhamnosus GG against fructose-induced fatty liver in mice. Mol Metab 2019;29:145–157.
42. Kahn BB, Alquier T, Carling D, Hardie DG. AMP-activated protein kinase: ancient energy gauge provides clues to modern understanding of metabolism. Cell Metab 2005;1:15–25.
43. Valentine RJ, Coughlan KA, Ruderman NB, Saha AK. Insulin inhibits AMPK activity and phosphorylates AMPK Ser485/491 through Akt in hepatocytes, myotubes and incubated rat skeletal muscle. Arch Biochem Biophys 2014;562:62–69.
44. van Zutphen T, Ciapaite J, Bloks VW, Ackereley C, Gerding A, Jurdzinski A, de Moraes RA, Zhang L, Wolters JC, Bischoff R, Wanders RJ, Houten SM, Bronte-Tinkew D, Shatseva T, Lewis GF, Groen AK, Reijngoud DJ, Bakker BM, Jonker JW, Kim PK, Bandsma RH. Malnutrition-associated liver steatosis and ATP depletion is caused by peroxisomal and mitochondrial dysfunction. J Hepatol 2016;65:1198–1208.
45. Hawley SA, Ross FA, Gowans GJ, Tibarewal P, Leslie NR, Hardie DG. Phosphorylation by Akt within the ST loop of AMPK-α1 down-regulates its activation in tumour cells. Biochem J 2014;459:275–287.
46. Gottlob K, Majewski N, Kennedy S, Kandel E, Robey RB, Hay N. Inhibition of early apoptotic events by Akt/PKB is dependent on the first committed step of glycolysis and mitochondrial hexokinase. Genes Dev 2001;15:1406–1418.
47. Pironi L, Joly F, Forbes A, Colomb V, Lyszkowska M, Baxter J, Gabe S, Hébuterne X, Gambarara M, Gottrand F, Cuerda C, Thul P, Messing B, Goulet O, Staun M, Van Gossum A. Home Artificial Nutrition & Chronic Intestinal Failure Working Group of the European Society for Clinical Nutrition and Metabolism (ESPEN). Long-term follow-up of patients on home parenteral nutrition in Europe: implications for intestinal transplantation. Gut 2011;60:17–25.
48. Wang Y, Ding WX, Li T. Cholesterol and bile acid-mediated regulation of autophagy in fatty liver diseases and atherosclerosis. Biochim Biophys Acta Mol Cell Biol Lipids 2018;1863:726–733.
49. Xu Z, Sun Y. The role of parenteral lipids in the development of hepatic dysfunction and hepatic steatosis in a mouse model of total parenteral nutrition. J Nutr Sci Vitaminol (Tokyo) 2019;65:24–30.
50. Wang H, Khaoustov VI, Krishnan B, Cai W, Stoll B, Burrin DG, Yoffe B. Total parenteral nutrition induces liver steatosis and apoptosis in neonatal piglets. J Nutr 2006;136:2547–2552.
51. Zhan L, Yang I, Kong B, Shen J, Gorczyca L, Memon N, Buckley BT, Guo GL. Dysregulation of bile acid homeostasis in parenteral nutrition mouse model. Am J Physiol Gastrointest Liver Physiol 2016;310:G93–G102.
52. Yang J, Sun H, Tian F, Wan S, Mamtawla G, Wang P, Gao X, Zhang L, Li J, Shen Y, Wang X. Autophagy suppression plays a role in parenteral nutrition-associated lung injury. Clin Nutr (Edinburgh, Scotland) 2021;40:560–570.
53. Zhang T, Yan J, Wang N, Dai L, Wang Y, Cai W. Autophagy may protect against parenteral nutrition-associated liver disease by suppressing endoplasmic reticulum stress. JPEN J Parenter Enteral Nutr 2019;43:96–106.
54. Hebbard L, George J. Animal models of nonalcoholic fatty liver disease. Nat Rev Gastroenterol Hepatol 2011;8:35–44.
55. Belli DC, Fournier LA, Lepage G, Yousef I, Roy CC. S-adenosylmethionine prevents total parenteral nutrition-induced cholestasis in the rat. J Hepatol 1994;21:18–23.
56. Li N, Zhang HH, Wang SH, Zhu WM, Ren JA, Li JS. S-adenosylmethionine in treatment of cholestasis after total parenteral nutrition: laboratory investigation and clinical application. Hepatobiliary Pancreat Dis Int 2002;1:96–100.
57. Martinez-Una M, Varela-Rey M, Mestre D, Fernandez-Ares L, Fresnedo O, Fernandez-Ramos D, Gutierrez-de Juan V, Martin-Guerrero I, Garcia-Orad A, Luka Z, Wagner C, Lu SC, Garcia-Monzon C, Finnell RH, Aurrekoetxea I, Buque X, Martinez-Chantar ML, Mato JM, Aspichueta P. S-Adenosylmethionine increases circulating very-low density lipoprotein clearance in non-alcoholic fatty liver disease. J Hepatol 2015;62:673–681.
58. King AL, Mantena SK, Andringa KK, Millender-Swain T, Dunham-Snary KJ, Oliva CR, Griguer CE, Bailey SM. The methyl donor S-adenosylmethionine prevents liver hypoxia and dysregulation of mitochondrial bioenergetic function in a rat model of alcohol-induced fatty liver disease. Redox Biol 2016;9:188–197.
59. Frau M, Feo F, Pascale RM. Pleiotropic effects of methionine adenosyltransferases deregulation as determinants of liver cancer progression and prognosis. J Hepatol 2013;59:830–841.
60. Sutter BM, Wu X, Laxman S, Tu BP. Methionine inhibits autophagy and promotes growth by inducing the SAM-responsive methylation of PP2A. Cell 2013;154:403–415.
61. Laxman S, Sutter BM, Tu BP. Methionine is a signal of amino acid sufficiency that inhibits autophagy through the methylation of PP2A. Autophagy 2014;10:386–387.
62. Mutanen A, Lohi J, Merras-Salmio L, Koivusalo A, Pakarinen MP. Prediction, identification and progression of histopathological liver disease activity in children with intestinal failure. J Hepatol 2021;74:593–602.
63. Sasdelli AS, Agostini F, Pazzeschi C, Guidetti M, Lal S, Pironi L. Assessment of intestinal failure associated liver disease according to different diagnostic criteria. Clin Nutr 2019;38:1198–1205.
64. Hirai H, Sootome H, Nakatsuru Y, Miyama K, Taguchi S, Tsujioka K, Ueno Y, Hatch H, Majumder PK, Pan BS, Kotani H. MK-2206, an allosteric Akt inhibitor, enhances antitumor efficacy by standard chemotherapeutic agents or molecular targeted drugs in vitro and in vivo. Mol Cancer Ther 2010;9:1956–1967.
65. Li G, Wang L, Jiang Y, Kong X, Fan Q, Ge S, Hao Y. Upregulation of Akt signaling enhances femoral fracture healing by accelerating atrophic quadriceps recovery. Biochim Biophys Acta Mol Basis Dis 2017;1863:2848–2861.

66. Sujobert P, Poulain L, Paubelle E, Zylbersztejn F, Grenier A, Lambert M, Townsend EC, Brusq JM, Nicodeme E, Decrooqc J, Nepstad I, Green AS, Mondesir J, Hospital MA, Jacque N, Christodoulou A, Desouza TA, Hermine O, Foretz M, Viollet B, Lacombe C, Mayeux P, Weinstock DM, Moura IC, Bouscary D, Tamburini J. Co-activation of AMPK and mTORC1 induces cytotoxicity in acute myeloid leukemia. Cell Rep 2015;11:1446–1457.
67. Kleiner DE, Brunt EM, Van Natta M, Behling C, Contos MJ, Cummings OW, Ferrell LD, Liu YC, Torbenson MS, Unalp-Arida A, Yeh M, McCullough AJ, Sanyal AJ, Nonalcoholic Steatohepatitis Clinical Research N. Design and validation of a histological scoring system for nonalcoholic fatty liver disease. Hepatology 2005;41:1313–1321.

Received November 18, 2021. Accepted May 18, 2022.

Correspondence
Address correspondence to: Xinying Wang, MD, PhD, Department of General Surgery, Jinling Hospital, Medical School of Nanjing University. 305 East Zhongshan Road, Nanjing, 210002, China. e-mail: wangxinying@nju.edu.cn; tel: +86-25-80861429. Bin Xue, PhD, LongMian Avenue, Nanjing 211166, China. tel: +86-25-87115542 e-mail: xuebin@njmu.edu.cn; or Chaojun Li, PhD, Hankou Road, Nanjing, 210093, China. tel: +86-25-83596289. e-mail: licj@nju.edu.cn.

CRediT Authorship Contributions
Gulisudmu Maitiabula (Performed experiments, analyzed data, and wrote the manuscript: Lead)
Feng Tian (Performed experiments and analyzed data: Equal)
Peng Wang (Helped perform animal and molecular biological experiments: Supporting)
Li Zhang (Helped perform histological staining: Supporting)
Xuejin Gao (Helped perform histological staining: Supporting)
Songlin Wan (Helped perform animal and molecular biological experiments: Supporting)
Haifeng Sun (Helped perform animal and molecular biological experiments: Supporting)
Jianbo Yang (Helped perform animal and molecular biological experiments: Supporting)
Yupeng Zhang (Helped perform animal and molecular biological experiments: Supporting)
Tingting Gao (Helped perform histological staining: Supporting)
Bin Xue (Helped design the project: Supporting)
Chaojun Li (Helped design the project: Supporting)
Jieshou Li (Helped design the project: Supporting)
Xinying Wang (Conceived and coordinated the study, designed, and supervised the study: Lead)

Conflicts of interest
The authors disclose no conflicts.

Funding
This study was supported by the National Natural Science Foundation of China (81470797, 81770531, 81700518, and 81900524), the Science Foundation of Outstanding Youth in Jiangsu Province (BK20170009), the National Science and Technology Research Funding for Public Welfare Medical Projects (201502022), "The 13th Five-Year Plan" Foundation of Jiangsu Province for Medical Key Talents (ZDRCA2016091), and Natural Science Foundation of Jiangsu Province (BK20170622).